Geochemistry Geophysics Geosystems G3
AN ELECTRONIC JOURNAL OF THE EARTH SCIENCES
Published by AGU and the Geochemical Society

Article
Volume 7, Number 5
3 May 2006
Q05004, doi:10.1029/2005GC001087
ISSN: 1525-2027

Interseismic strain accumulation: Spin-up, cycle invariance, and irregular rupture sequences

E. A. Hetland
Department of Earth, Atmospheric and Planetary Sciences, Massachusetts Institute of Technology, Cambridge, Massachusetts 02139, USA

Now at Seismological Laboratory, MC 252-21, California Institute of Technology, 1200 East California Boulevard, Pasadena, California 91125, USA (eah@gps.caltech.edu)

B. H. Hager
Department of Earth, Atmospheric and Planetary Sciences, Massachusetts Institute of Technology, Cambridge, Massachusetts 02139, USA

[1] Using models of infinite length strike-slip faults in an elastic layer above linear viscoelastic regions, we investigate interseismic deformation. In the models we investigate, interseismic strain accumulation on mature faults is the result of the cumulative effects of all previous ruptures and is independent of the fault loading conditions. The time for a fault to spin-up to a mature state depends on the rheologies and the fault loading conditions. After the model has spun-up, the temporal variation of shear stresses is determined by the fault slip rate and model rheologies. The change in stress during spin-up depends on the slip rate, rheologies, and fault loading conditions but is independent of the magnitude of the initial stress. Over enough cycles such that the cumulative deformation is block-like, the average mature interseismic velocities are equal to the interseismic velocities of an elastic model with the same geometry and distribution of shear moduli. In a model that has spun-up with the fault rupturing periodically, the cumulative deformation is block-like at the end of each seismic cycle, and the interseismic deformation is cycle-invariant (i.e., the same in all cycles). When the fault ruptures nonperiodically, the fault spins up to a mature state that is the same as if the fault had ruptured periodically with the mean slip rate. When the fault slip rate within each cycle varies, the interseismic deformation evolves toward the cycle-invariant deformation determined by the most recent fault slip rate. Around a fault whose slip rate has been faster (slower) than average, interseismic velocities are larger (smaller) than the cycle-invariant velocities and increase (decrease) from cycle to cycle.

Components: 14,607 words, 15 figures.

Keywords: fault spin-up; interseismic strain accumulation; interseismic velocities; rupture clustering.

Index Terms: 1207 Geodesy and Gravity: Transient deformation (6924, 7230, 7240); 1242 Geodesy and Gravity: Seismic cycle related deformations (6924, 7209, 7223, 7230); 8120 Tectonophysics: Dynamics of lithosphere and mantle: general (1213).

Received 26 July 2005; **Revised** 30 November 2005; **Accepted** 27 January 2006; **Published** 3 May 2006.

Hetland, E. A., and B. H. Hager (2006), Interseismic strain accumulation: Spin-up, cycle invariance, and irregular rupture sequences, *Geochem. Geophys. Geosyst.*, *7*, Q05004, doi:10.1029/2005GC001087.

1. Introduction

[2] There have been many studies of geodetically observed interseismic deformation [e.g., *Savage and Burford*, 1973; *Bourne et al.*, 1998; *Peltzer et al.*, 2001; *Pollitz*, 2003b; *Johnson and Segall*, 2004; *Smith and Sandwell*, 2004; *Meade and Hager*, 2005a; *Pollitz and Nyst*, 2005]. In this paper, we define interseismic deformation as any deformation during the earthquake cycle that does not include the coseismic deformation due to the fault rupture. Transient deformation observed from weeks to decades following a fault rupture is often referred to as postseismic deformation; we include this postseismic deformation as part of the interseismic deformation. (Note, however, that interseismic deformation is often used to refer only to the relatively steady motion that occurs after the postseismic transient has decayed.) Geodetic observations (e.g., Global Positioning System, radar interferometry) of interseismic deformation represent a snapshot of the deformation throughout the *seismic cycle*, and thus detect instantaneous deformation [e.g., *Pollitz*, 2003a].

[3] One of the main scientific goals for interpreting observed interseismic deformation is to constrain the rheology of the continental lithosphere [e.g., *Hetland and Hager*, 2003; *Pollitz*, 2003b; *Freed and Bürgmann*, 2004; *Johnson and Segall*, 2004]; however, accurate interpretations of interseismic deformation can also have a large impact on society. An accurate model of observed interseismic deformation can provide crucial information on the rupture potential of faults [e.g., *Dolan et al.*, 1995; *Meade and Hager*, 2005b]. However, observations of interseismic deformation must be put into the context of a strain accumulation model appropriate for that fault. In this paper, we illustrate how strain accumulation is related to prior fault activity, mechanisms of *fault loading*, and viscoelastic rheologies. (Italicized terms are defined in the glossary, which follows the main text.)

1.1. Linear Rheologies of Strain Accumulation Models

[4] All models of interseismic deformation assume a rheology of the lithosphere. The simplest rheologies are either linear elastic or viscous. An elastic rheology or is represented conceptually by the mechanical analogue model of a spring, while a viscous rheology is represented by a dashpot. Combining a spring and a dashpot element in series produces a Maxwell rheology, the most commonly assumed viscoelastic rheology. The Maxwell rheology is capable of instantaneous elastic strain, followed by a single phase of nonrecoverable viscous creep. A Kelvin element is formed by combining a spring and dashpot in parallel, and the viscous relaxation of the Kelvin element is recoverable. Multiviscous rheologies can be built by combining a Maxwell element in series with one or more Kelvin elements. For instance, the biviscous Burgers rheology is the combination of a Maxwell element with one Kelvin element in series.

[5] A prominent interpretation of interseismic deformation assumes that elastic strains are unimportant in geodetic data and that the deformation at the surface is a replica of the deformation at depth [e.g., *Bourne et al.*, 1998]. This approach uses a purely viscous rheology for the lithosphere, only considering a dashpot element. Numerous studies have shown, however, that the elastic component of the lithosphere's rheology is important and that deformation at the surface is a record of strain accumulation on active faults [e.g., *Li and Rice*, 1987; *Savage*, 1990; *Roy and Royden*, 2000; *Hetland and Hager*, 2004, 2005].

1.2. Classic Elastic Half-Space Model

[6] The classic model of strain accumulation is that of *Savage and Burford* [1973], in which an infinite-length strike-slip fault is loaded by steady sliding on the down-dip extension of the fault in an elastic half-space (Figure 1a). This model, which we refer to as the *classic elastic half-space model* (CEHM), considers the elastic response to slip on the fault using only the spring in a Maxwell element. The velocities at the surface in the CEHM are constant during the interseismic period and are given by

$$v(x) = \frac{v_T}{\pi} \tan^{-1} \frac{x}{D}, \tag{1}$$

where x is the distance from the fault, D is the *locking depth* and v_T is the rate of sliding of the deep fault. Since the far-field is driven by the steady sliding at depth, v_T is the difference in the far-field velocities across the fault. The velocities of the CEHM are identical to the difference between block-like displacements across the fault and the coseismic displacements, divided by the rupture repeat time [*Savage and Burford*, 1973].

[7] The CEHM can be extended to all types of faults and is the basis of block models [e.g., *Meade and Hager*, 2005a]. Because of the use of the CEHM, block models assume that the continental

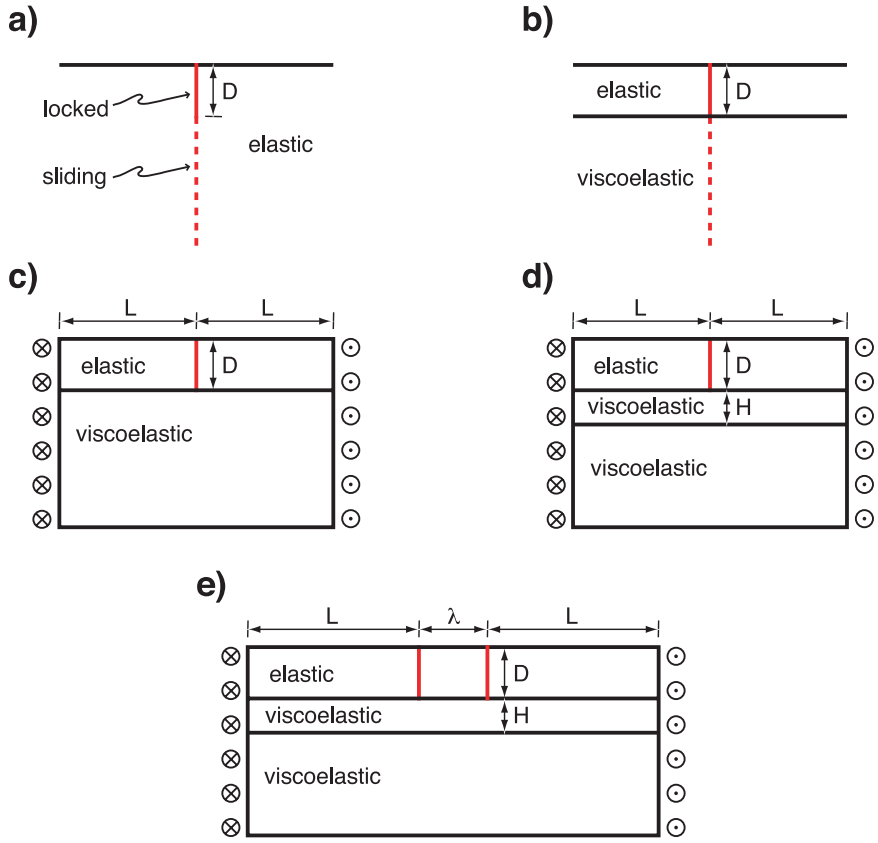

Figure 1. Cartoons of the models considered in this paper (solid and dashed red lines indicate the interseismically locked and sliding portions of the fault; circles containing dots and crosses indicate velocity boundary conditions into and out of the page): (a) the classic elastic half-space model, (b) an elastic layer over a viscoelastic half-space (a one-layer model) with the fault loaded by steady sliding at depth, (c) a one-layer model driven by far-field shear, (d) an elastic layer over a viscoelastic layer and lower viscoelastic half-space (a two-layer model) driven by far-field shear, and (e) and a two-layer model with two faults. See Appendix A for a discussion of the height of the bounded models.

lithosphere behaves elastically over seismic cycle timescales and that v_T is steady in time. However, inelasticity of the continental lower crust and mantle must be considered in order to describe observations of postseismic deformation [e.g., *Ivins*, 1996; *Hearn et al.*, 2002; *Pollitz*, 2003b; *Freed and Bürgmann*, 2004], and fault *slip rates* are often nonsteady over timescales of hundreds to thousands of years [e.g., *Sharp*, 1981; *Wallace*, 1987; *Grant and Sieh*, 1994; *Weldon et al.*, 2004].

1.3. Standard Viscoelastic Model

[8] In a seminal paper, *Savage and Prescott* [1978] extended the CEHM to a model of an elastic layer overlying a Maxwell viscoelastic half-space (Figure 1b), including the response of both the dashpot and spring of the Maxwell element to ruptures in the upper elastic layer. Their solution, which we refer to as the *standard model of interseismic deformation*, gives the time-dependent deformation throughout a mature seismic cycle in a periodic *rupture sequence*. A periodic rupture sequence is one in which all fault ruptures occur regularly in time with constant offset, while a mature cycle is such that the deformation within the cycle does not depend on the number of previous ruptures (often referred to as steady state). The standard model is based on the image solution of *Rybicki* [1971], and thus the interseismic deformation through time is expressed as perturbations to the model of *Savage and Burford* [1973]. The standard model was rederived by *Savage and Lisowski* [1998] and *Savage* [2000], and most modern calculations of the standard models are done using one of these later formulations.

[9] The standard model is parameterized by the parameter τ_o, often referred to as the *Savage parameter*. The Savage parameter was first intro-

duced by *Savage and Prescott* [1978] as $\tau_o = T/2\tau_M$, where T is the seismic repeat time and $\tau_M = \eta_M/\mu_M$ is the material relaxation time of the lower Maxwell viscoelastic half-space with viscosity η_M and shear modulus μ_M. Elsewhere we have extended the definition of the Savage parameter to models with general linear viscoelastic rheologies and clarified its definition as the ratio of the seismic repeat time to a mechanical timescale associated with the coupling of the uppermost layer to the viscoelastic region below [*Hetland and Hager*, 2005]. In general the Savage parameter is given by $\tau_o = T_o|\alpha_1|$, where T_o is the nominal repeat time and $|\alpha_1|^{-1}$ is a mechanical relaxation time [*Hetland and Hager*, 2005]. For models of a fault in an upper elastic layer overlying a lower Maxwell viscoelastic region, there is only one time scale. When either the upper layer is viscoelastic or the lower region has more than one viscous phase, there are multiple mechanical time scales [e.g., *Hetland and Hager*, 2005]. As a result, τ_o is defined uniquely only for models of an elastic layer over a Maxwell region. For all other models, we specify the mechanical relaxation time used in the definition of τ_o. When the relaxation time of the model is much longer than the nominal repeat time, τ_o is low, whereas when the relaxation time is shorter than the repeat time, τ_o is high.

[10] The standard model is widely used to gain insight into interseismic deformation [e.g., *Savage*, 1990; *Meade and Hager*, 2004], as well as to interpret geodetic observation [e.g., *Segall*, 2002; *Dixon et al.*, 2003; *Hilley et al.*, 2005]. *Johnson and Segall* [2004] incorporated viscous fault slip into the standard model, while *Hetland and Hager* [2005] generalized the analysis of Savage and coworkers in order to extend the standard model to general linear viscoelastic rheologies and irregular earthquake sequences.

1.4. Alternative Models of Strain Accumulation

[11] Interseismic deformation given in terms of perturbations to a CEHM is often assumed to hold only for models in which the fault is loaded by steady sliding of the down-dip extension of the fault [e.g., *Bowman et al.*, 2003]. Rejecting steady sliding of the fault at depth, researchers have interpreted localized interseismic strain observed across faults is to imply that strain is also localized at depth [e.g., *Bourne et al.*, 1998; *Jackson*, 2002] or that the lithosphere is weaker near the fault compared to the surrounding regions [e.g., *Pollitz*, 2001; *Pollitz and Nyst*, 2005].

[12] Localized interseismic strain has also been interpreted to be due largely to postseismic transients from only the most recent earthquakes, while simple and/or pure shear loads the fault [e.g., *Vergnolle et al.*, 2003; *Freed and Bürgmann*, 2004; *Pollitz and Nyst*, 2005]. If a fault has never ruptured, but has been loaded by far-field shear, then the appropriate model after the first rupture is that of the postseismic response due to the most recent rupture plus simple shear. Additionally, if the relaxation timescales of the lithosphere are much shorter than the seismic repeat time, then the interseismic velocities before a rupture are those of simple shear [e.g., *Savage and Prescott*, 1978], and the postseismic deformation can be modeled ignoring all but the last rupture. Finally, when the transient deformation from the most recent rupture varies much faster than the cumulative postseismic effects of all but the last rupture, the interseismic velocities observed immediately before the last rupture can approximate the cumulative effects of the previous ruptures throughout the postseismic period [e.g., *Bürgmann et al.*, 2002; *Hearn et al.*, 2002].

1.5. Overview of the Paper

[13] In this paper, we demonstrate the effects of fault rupture activity and rheology on interseismic deformation, using viscoelastic models with infinite-length strike-slip faults. With these simple 2D models, we construct a framework for understanding the evolution of interseismic deformation as a fault model matures, as well as during times of nonperiodic fault activity. In section 2, we show that a model with a fault that ruptures repeatedly will eventually approach a final *mature state*, and also show that while the initial deformation depends on the particular fault loading conditions, the mature deformation does not as long as fault loading is constant in time. In section 2, we also address the dependence of the time for a fault model to mature on the parameters of several simple models. In section 3, we discuss the variation of interseismic deformation during periods when the fault rupture activity is not periodic, and we show that when the slip rate of the fault has been recently faster (slower) than the long-term average, the interseismic velocities are consistently faster (slower) than those within periodic seismic cycles. In section 4, we consider the *spin-up* and mature interseismic deformation in models with

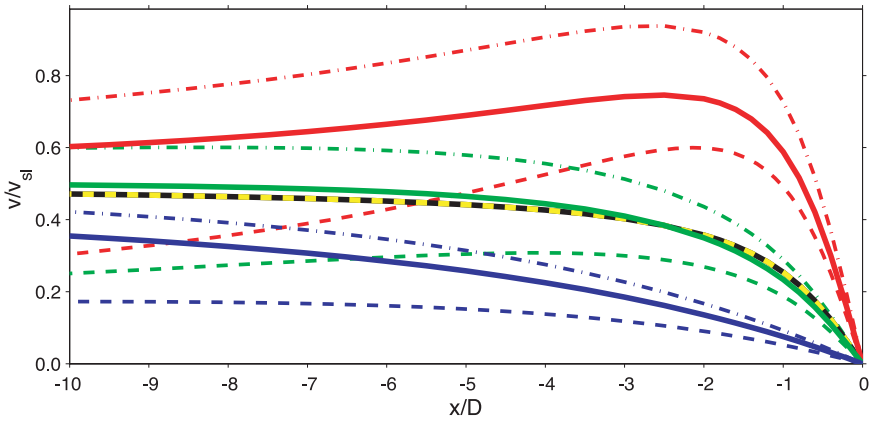

Figure 2. Cycle-invariant velocities (solid lines) and the velocities following the first rupture on a fault rupturing periodically in an elastic layer over a Maxwell viscoelastic half-space ($\tau_o = 10$) loaded by simple shear (dashed lines) and from below (dash-dot lines) at times $0.1T$ (red), $0.4T$ (green), and $0.9T$ (blue). For reference, the primary velocities are also shown (black-yellow dashed line).

two parallel strike-slip faults, and demonstrate that when the slip rates on the two faults change, the interseismic velocities again systematically change, as in the single fault models. We follow these sections with a discussion of the results of this paper and brief conclusions. For reference, a notation list and a brief glossary of terms used throughout this paper appear at the end of the paper.

[14] Throughout this paper, we consider the dependence of the interseismic deformation on the fault loading conditions. Models where strain at depth is localized or is distributed are two end-member models of deep deformation driven by two configurations of fault loading conditions. For the first model, the fault is loaded by steady sliding on the fault below the locking depth, similar to the fault loading of the CEHM and the standard model (Figure 1b) [e.g., *Savage and Burford*, 1973; *Savage and Prescott*, 1978]. We use the analytic model of *Hetland and Hager* [2005] to calculate the deformation of all models driven purely by steady sliding at depth. A more realistic model is that of a fault loaded by far-field shear boundary conditions, where the deformation at great depth is that of simple shear (Figures 1c–1e) [e.g., *Bonafede et al.*, 1986; *Lyzenga et al.*, 1991; *Pollitz*, 2001; *Hetland and Hager*, 2004]. We compute the deformation of all fault models driven by far-field shear using the finite element program GeoFEST [*Lyzenga et al.*, 2000] (see Appendix A for the finite element model details).

[15] Infinite-length faults are obviously not appropriate for Earth, and 3D effects are important for models of interseismic deformation [e.g., *Chèry et al.*, 2001; *Lynch et al.*, 2003; *Smith and Sandwell*, 2004]. Nevertheless, these two-dimensional models give appreciable insight into models of strain accumulation. We specify the time and magnitude of fault ruptures in order to construct specific fault rupture sequences, an approach similar to that of *Meade and Hager* [2004]. *Meade and Hager* [2004] considered the effect on interseismic velocities for only one nonperiodic fault history function, and we consider the evolution of interseismic velocities and stresses during more general nonperiodic rupture sequences. All of the faults in our models are right-lateral. Models containing one fault are antisymmetric, and we only show the positive displacements and velocities.

2. Fault Spin-Up and Cycle Invariance

[16] At all times, interseismic surface deformation depends on the model geometries and rheologies. The surface deformation also depends on the fault loading conditions and the number of previous ruptures; however, after a sufficient number of ruptures in a periodic rupture sequence, the surface deformation no longer depends on the loading conditions or the rupture history [e.g., *Li and Rice*, 1987; *Hetland and Hager*, 2004]. This final state is often referred to as a steady or a mature state. The term "steady state" is misleading, as the interseismic deformation is not, in general, steady in time, but, for some parameters, can vary rapidly throughout a seismic cycle. On the other hand, the term "mature state" does not imply that the deformation is steady, and is a more appropriate term. When the rupture sequence is periodic, the mature interseis-

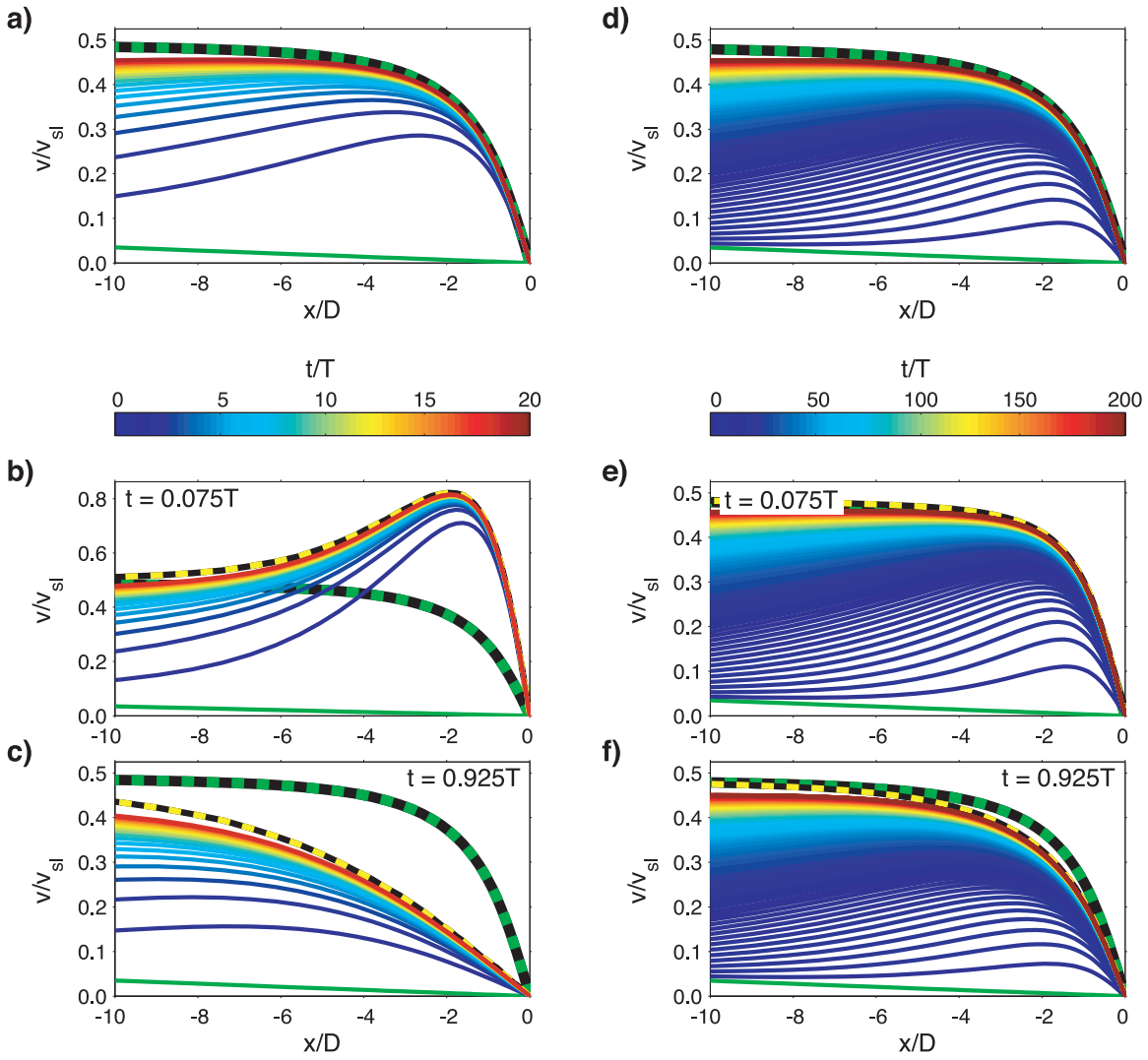

Figure 3. Interseismic velocities as initially unstressed, two-layer models with Maxwell viscoelastic rheologies ($\alpha_2/\alpha_1 = 1.5$, $\tau_{hs}/\tau_{ml} = 5$, and $\tau_o = 10$ (a–c) or 1 (d–f)) spin-up to a mature state with periodic ruptures, with the fault loaded by simple shear applied at $x = \pm 120D$. (a and d) Average interseismic velocities in each seismic cycle up to cycle N_i (line color indicates cycle number according to the color scale below each panel). Also shown are the initial velocities (green) and the primary velocities (green-black dashed line). (b and e) Interseismic velocities in each seismic cycle up to cycle N_i at time $0.075T$. Line color is cycle number as above, yellow-black and green-black dashed lines are the cycle-invariant and primary velocities, respectively, and green lines are the initial velocities. (c and d) Interseismic velocities in each seismic cycle at time $0.925T$. Primary velocities and line style are as in Figures 3b and 3e.

mic deformation is the same in every cycle, hence we say that the deformation is cycle-invariant or that the system is in a *cycle-invariant state*. In this paper, we often refer to cycle-invariant velocities as just invariant velocities (likewise for stresses), and we refer to a cycle-invariant state as cycle invariance. The time for a fault model to reach a mature state is referred to as the spin-up time, or sometimes the cycle-up time. In this section, we discuss the transition from the initial to the mature deformation, describe the mature interseismic deformation, and characterize fault spin-up.

2.1. Transition From Initial to Mature Interseismic Deformation

[17] When the fault is loaded by steady sliding on the extension of the fault below the interseismically locked portion (Figure 1b), the initial surface displacements are given by an inverse tangent function [e.g., *Rybicki*, 1971]. After a sufficient number

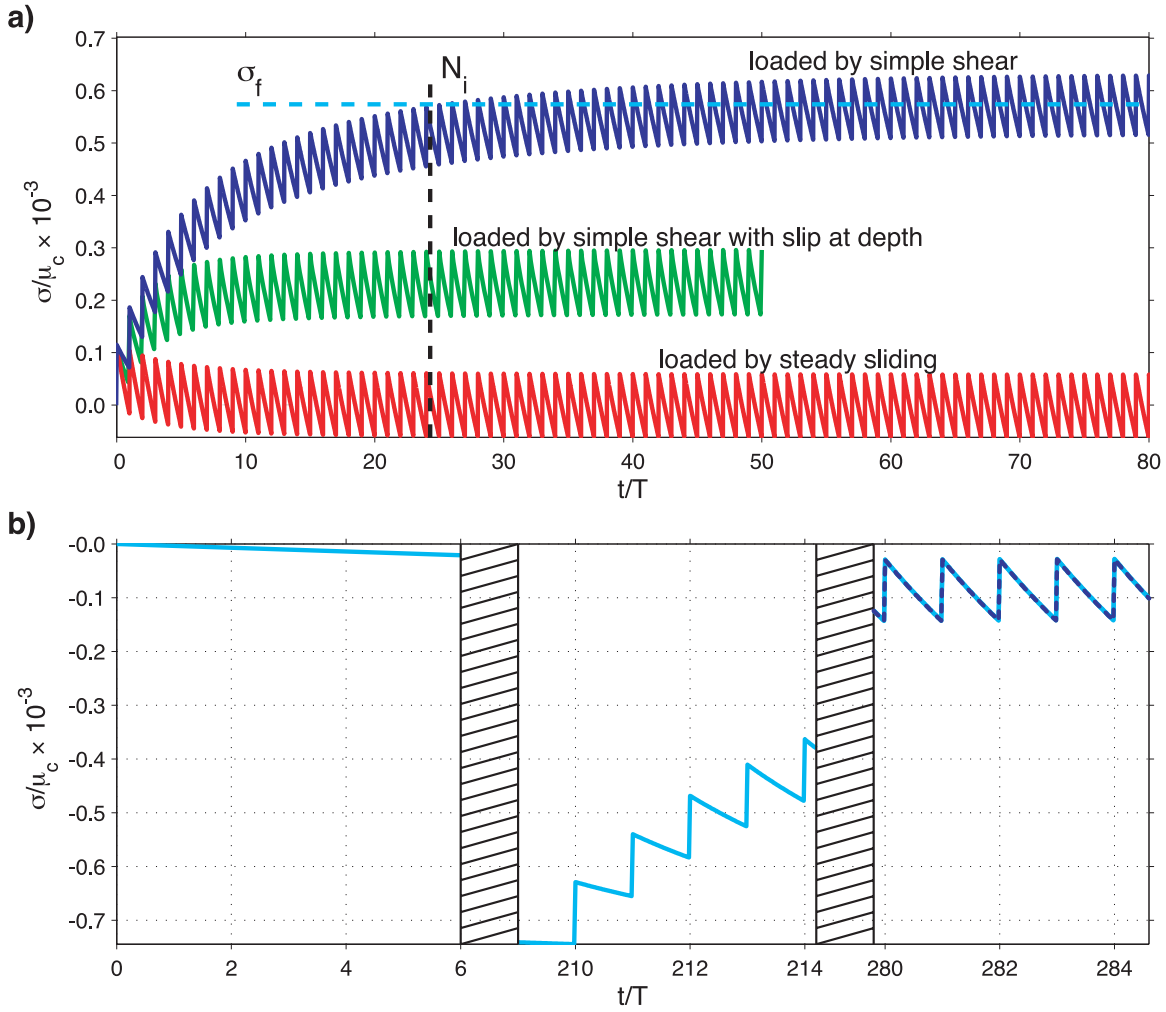

Figure 4. (a) Shear stress on the fault near the surface as three initially unstressed, one-layer, Maxwell viscoelastic models ($\tau_o = 0.35$) loaded differently spin-up to cycle-invariant states, also shown are N_i and σ_f for the model driven by simple shear boundary conditions. (b) Shear stress on a fault that is loaded by far-field shear for $210T$ before the first fault rupture (cyan line) and the cycle-invariant stresses, arbitrarily offset, of the same model initially unstressed (blue dashed line). Hatched regions indicate time periods not shown.

of ruptures in a periodic sequence, the amount of stress relaxation equals the loading rate, and, due to the construction of this model with the back-slip method, the cycle-invariant velocities are lower than those preceding the first several ruptures (Figure 2) [*Hetland and Hager*, 2005].

[18] In the case of a fault loaded by far-field shear, before the fault ruptures, the velocities across the fault are those of simple shear, a replica of the velocities at depth (Figure 3). Following the first several ruptures, the velocities increase as the postseismic transients accumulate (Figure 3). As in the first end-member model, after a sufficient number of periodic ruptures, the interseismic deformation becomes cycle-invariant, with the invariant velocities larger than the initial (Figures 2 and 3). In both end member models, during cycle invariance the interseismic velocities can be characterized as perturbations to the CEHM [e.g., *Savage and Prescott*, 1978; *Hetland and Hager*, 2005].

[19] In general, the number of cycles it takes to reach cycle invariance scales inversely with the Savage parameter (τ_o). During each cycle the shear stresses on the fault vary, and as the model spins up to a cycle-invariant state, the stresses evolve from cycle to cycle (Figure 4a). The average mature shear stresses depend on the fault slip rate, rheologies, fault loading, and the magnitudes of the initial stresses. For linear rheologies, the change

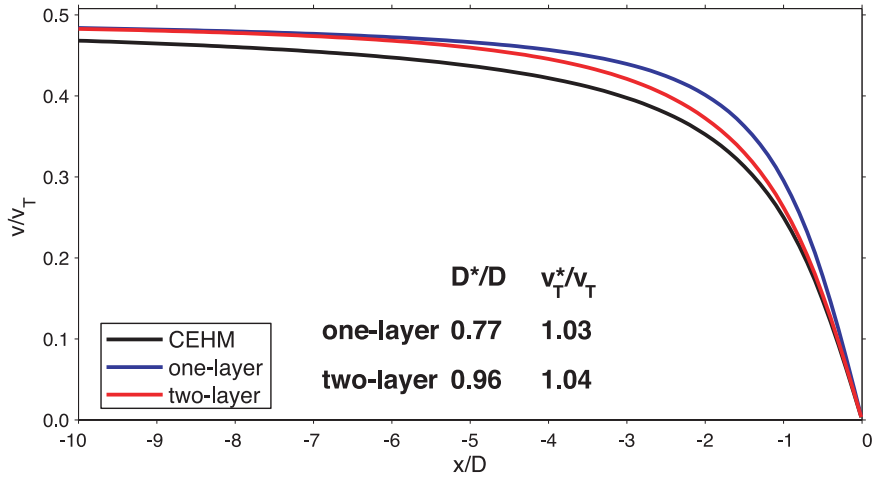

Figure 5. Interseismic velocities for elastic models with locking-depth and fault loading rate D and v_T, respectively. CEHM has a uniform elastic shear modulus, while the one- and two-layer models have a half-space with shear modulus 2 μ, where μ is the shear modulus of the upper layers. D^* and v_T^* are the apparent locking depths and loading rates from the best fit CEHM to the velocities of the one- and two-layer models.

in stress during spin-up is independent of the initial stresses (Figure 4b). We define σ_f to be the total change in the shear stress on the fault near the surface, and if we assume that the model is initially unstressed, σ_f is the average mature shear stress.

[20] The amount that the stress changes during spin-up scales with τ_o^{-1}, as well as with the rupture magnitude. The stresses on the fault asymptotically approach σ_f, and we take the time when the average stress throughout a seismic cycle reaches 0.9 σ_f to be the spin-up time, t_i. We nondimensionalize time by the rupture repeat time, T, so that $N_i = t_i/T$ is the number of ruptures necessary for the deformation to become nearly cycle-invariant (Figure 4a). During cycle N_i, the interseismic velocities are close to the invariant velocities near the fault; however, farther from the fault, the velocities are not the invariant velocities until later when the average interseismic stress on the fault is closer to σ_f (Figure 3). In section 2.4, we will quantify how N_i and σ_f depend on the parameters of several model geometries and rheologies.

2.2. Dependence of Spin-Up on Fault Loading

[21] The time that it takes a model to reach a mature state depends not only on the model rheologies, but also on fault loading conditions. We demonstrate the dependence on the fault loading by spinning up three models of a fault in an upper layer over a viscoelastic half-space (one-layer models; Figure 4a). Two of the three models have identical rheologies, and in the first model the fault is loaded by far-field boundary conditions, while in the second the fault is loaded by deep, steady sliding. The third model is a modification of the first two by the addition of a viscously weak column extending from two locking depths below the surface to the bottom of the model. The weak column accommodates postseismic stress relaxation and there is secular shear across the column driven by a block-like basal boundary condition. In this model, slip across the weak zone is not steady in time and the fault is loaded by a combination of slip on the weak zone and far-field shear. We use the finite element method to compute the deformation of the third model, which has been described in detail by *Hetland and Hager* [2004]. The model driven by far-field shear takes the longest time to reach invariance, whereas the model driven by a combination of far-field shear and deep sliding is the fastest (Figure 4a). When the fault is loaded only by far-field shear, the spin-up time reflects the time required to diffuse postseismic stress far from the fault, so that the velocities in the far-field increase from those of simple shear to the cycle-invariant velocities (Figure 3). In the model driven by both far-field shear and deep slip, the far-field velocities build up to the invariant velocities quickly, due to the additional component of relaxation on the lower weak zone and the development of block-like deformation at depth. Finally, when the fault is loaded purely from below, the total change in shear stress on the fault during the spin-up is opposite in sign to when the fault is loaded by far-

field shear only, reflecting that the invariant displacements are lower than the initial when loaded by steady sliding at depth (Figure 2).

2.3. Mature Interseismic Deformation and Primary Velocities

[22] In a viscoelastic model with uniform elastic shear moduli and periodic ruptures, the average mature interseismic velocities across the fault are identical to those of the classic elastic half-space model (CEHM) of *Savage and Burford* [1973]. When the shear modulus is not uniform in the elastic model, the interseismic velocities are slightly different than those of the CEHM [*Rybicki*, 1971; *Chinnery and Jovanovich*, 1972]. For an elastic model with a depth-dependent shear modulus, the velocities resemble those of a CEHM, and we refer to D and v_T of the best fit CEHM as the apparent locking depth and velocity, respectively. When the shear modulus increases with depth, stains are larger across the fault, resulting in a lower apparent locking depth (Figure 5). Alternatively a model with decreasing shear modulus yields a higher apparent locking depth.

[23] In a viscoelastic model with periodic ruptures, the average cycle invariant velocities are equal to those of an elastic model with the same elastic shear modulus structure as the viscoelastic model; we refer to this case as the *equivalent elastic model*. We refer to the average interseismic velocities as the *primary velocities*, and thus the velocities of the equivalent elastic model are the primary velocities. The degree of perturbation to the primary velocities throughout a seismic cycle is determined by the rheologies and the rupture history. As the relaxation timescales of the model become much larger than the rupture repeat time, the perturbations to the primary velocities become negligible and the interseismic deformation is close to that of the equivalent elastic model at all times throughout the seismic cycle (Figures 3e and 3f); hence the primary velocities can be thought of as the limit of a viscoelastic model as the Maxwell viscosity becomes large [e.g., *Savage and Prescott*, 1978].

[24] For a periodic rupture sequence, the average invariant velocities throughout a seismic cycle are the primary velocities for all model rheologies as long as the fault loading is steady in time. This is a consequence of the fact that the far-field deforms the same amount as the near field over one complete seismic cycle, which includes the interseismic period and one rupture. In other words, the deformation at the end of a seismic cycle is block-like, with the difference between block-like displacements and the coseismic displacements being made up during the interseismic period.

2.3.1. Phase Variables of Interseismic Velocities

[25] Interseismic velocities can be described by the apparent D and v_T of a CEHM fit to the velocities, and thus D and v_T can be considered as *phase variables of the interseismic velocities*. When the shear modulus is uniform throughout the model, a CEHM fit to the primary velocities will yield the actual values of D and v_T; however, when the shear modulus is not uniform, D and v_T vary from the model locking depth and slip rate due to the difference in elastic structure (Figure 5); however, as the rheology does not change, the difference in the phase variables is the same at all times. A larger apparent locking depth results in smaller predicted strains across the fault, whereas a smaller apparent locking depth results in larger strains; hence there is a tradeoff between the locking depth and the velocity of the best fit CEHM.

[26] Immediately after a rupture in a periodic rupture sequence, the apparent D and v_T of the cycle-invariant interseismic velocities are lower and higher, respectively, than those of the primary velocities due to the large strains across the fault from the heightened postseismic velocities. Alternatively, late in the cycle, the apparent D of the invariant velocities is larger than that of the primary velocities, reflecting lower strains preceding the next rupture. When there is appreciable postseismic relaxation, the CEHM does not fit the interseismic velocities well at all times. The variation of the phase variable v_T throughout the cycle depends on the wavelength of deformation and the distance range considered; however the variation of the phase variable D adequately reflects the variation of strains across the faults throughout the seismic cycles.

2.4. Relations of Spin-Up Time and Stress Change

[27] As stated above, both N_i and σ_f depend on the fault loading conditions and rheologies. We determine relations of N_i and σ_f to model parameters only for faults loaded by far-field shear or by steady slip on the extension of the fault below the locking depth. We consider multiple models with both univiscous and biviscous viscoelastic rheologies, and we consider two model geometries:

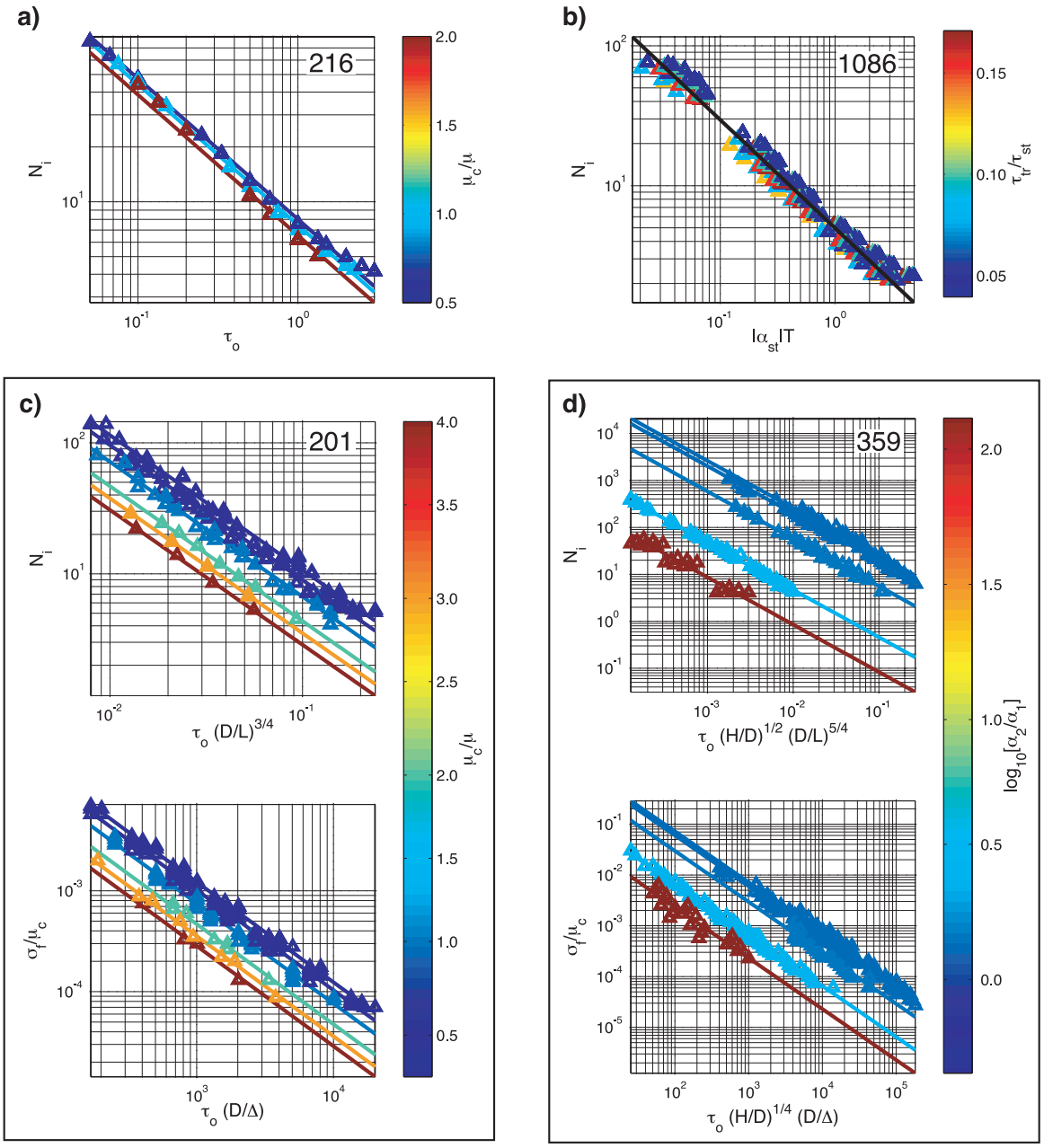

Figure 6. Number of ruptures required to approach a cycle-invariant state (N_i) for one-layer models with (a) a lower Maxwell viscoelastic half-space and (b) Burgers viscoelastic half-space in which the fault is loaded by steady-sliding on the extension of the fault at depth, (c) a one-layer model with a lower Maxwell half-space in which the fault is loaded by far-field shear, and (d) a two-layer model with a Maxwell viscoelastic middle layer and lower half-space in which the fault is loaded by far-field shear. The number of model realizations is indicated in each plot, and all variables are defined in the notation list. Also plotted is the change in shear stress on the fault during spin-up (σ_f) for a one-layer model (Figure 6c) and a two-layer model (Figure 6d), both with Maxwell rheologies and with the fault loaded by far-field shear.

an elastic layer over a viscoelastic half-space (the one-layer model; Figures 1b and 1c) and an elastic layer over a viscoelastic middle layer and half-space (the two-layer model; Figure 1d).

[28] For the case of an elastic layer over a linear viscoelastic half-space (a one-layer model, where the shear modulus of the upper layer and lower half-space is μ_c and μ, respectively) with the fault

loaded by steady sliding on the extension of the fault at depth,

$$N_i = A[\chi]\tau_o^{-m}, \tag{2}$$

where $A[\chi]$ are factors that depend on the rheological parameters and we determine m empirically. For a Maxwell viscoelastic lower half-space, we include a dependence on $\chi = \mu_c/\mu$ because time only scales for a constant contrast of shear moduli [*Hetland and Hager*, 2005]. For models with a Burgers viscoelastic lower half-space, $\chi = \tau_{tr}/\tau_{st}$, where $\tau_{tr} = |\alpha_{tr}|^{-1}$ and $\tau_{st} = |\alpha_{st}|^{-1}$ are the fastest and slowest mechanical time scales associated with a Burgers one-layer model [*Hetland and Hager*, 2005]. We only consider Burgers rheologies in which the recoverable Kelvin relaxation phase is weaker than the nonrecoverable Maxwell phase. We spun-up 216 Maxwell and 1,086 Burgers models, and fit the above scaling relation to determine $m \approx 3/4$ for both rheologies (Figures 6a and 6b). The scaling in the Maxwell models is slightly dependent on μ_c/μ, although the difference in $A[\chi]$ is within the scatter of the model spin-up times (Figure 6a). When $\tau_o = |\alpha_{tr}|T$ in a Burgers model, $A[\tau_{tr}/\tau_{st}]$ varies systematically over about one half an order of magnitude, whereas when $\tau_o = |\alpha_{st}|T$, A is roughly constant with little to no systematic variation with τ_{tr}/τ_{st}. Hence spin-up time is roughly constant for a given steady-state relaxation timescale, regardless of the transient timescales, implying that, to a large extent, the nonrecoverable, steady relaxation phase dominates the spin-up of the fault (i.e., $|\alpha_1| = |\alpha_{st}|$ for a one layer model with Burgers rheologies).

[29] For a one-layer model with a Maxwell viscoelastic lower half-space, where the fault is loaded by far-field boundary conditions, N_i also scales with the distance to the model edges where the boundary conditions are imposed. The extra length scale is because it is necessary to diffuse stresses, and hence transient deformation, to the boundaries in order to build up the velocities in the far-field to the invariant velocities (Figure 3). We spun up 201 models, with various model widths, rheologies, rupture repeat times, and rupture magnitudes, to determine the relations

$$N_i = A[\mu_c/\mu]\left(\frac{L}{D}\right)^{3/4}\tau_o^{-1} \tag{3}$$

and

$$\sigma_f/\mu_c = B[\mu_c/\mu]\left(\frac{\Delta}{D}\right)\tau_o^{-1}, \tag{4}$$

where L is the distance from the fault to the boundaries, Δ is the rupture offset, and we rounded the power of L/D to a rational fraction (Figure 6c). For a model with a fault in an upper elastic layer overlying a Maxwell viscoelastic layer and Maxwell viscoelastic half-space (a two-layer model), loaded by far-field shear,

$$N_i = A[\alpha_2/\alpha_1]\left(\frac{D}{H}\right)^{1/2}\left(\frac{L}{D}\right)^{5/4}\tau_o^{-1} \tag{5}$$

and

$$\sigma_f/\mu_c = B[\alpha_2/\alpha_1]\left(\frac{D}{H}\right)^{1/4}\left(\frac{\Delta}{D}\right)\tau_o^{-1}, \tag{6}$$

where H is the thickness of the middle viscoelastic layer, $\tau_o = |\alpha_1|T$, α_1 and α_2 are the coupling coefficients between the upper layer and the middle layer to the lower half-space (Appendix B), and we determined the powers in these relations by considering 359 model realizations (Figure 6d).

2.5. Spin-Up of a Nonperiodic Rupture Sequence

[30] A model with nonperiodic fault ruptures will also spin-up to a mature state. When the fault rupture history is random, with mean repeat times and rupture magnitudes T_o and Δ_o, respectively, the change in shear stress on the fault during spin-up is as if the fault had spun up while rupturing periodically with T_o and Δ_o (Figure 7a). For nonperiodic ruptures, σ_f is the difference between the initial shear stress and the average stress on the fault over a time window sufficiently long such that the variations of T and Δ average out to T_o and Δ_o. Over this time window, the cumulative deformation is block-like and the average interseismic velocities are the primary velocities (Figure 7b). For example, in a model with a fault rupture history composed of repeating a nonperiodic elementary sequence of N ruptures, the change in shear stresses on the fault and the average interseismic velocities over the elementary sequence are equal to σ_f and the primary velocities, respectively.

[31] The time for a model to spin-up to a mature state does not depend on the rupture repeat time, T, since $N_i = \frac{t_i}{T} \sim \tau_o^{-1} = \frac{1}{|\alpha_1|T}$. As the spin-up time of a model only depends on the rheologies and the model geometry, the spin-up time can be considered to be the time required for a fault model to adjust to the imposition of fault loading conditions. On the other hand, the change in shear stress on

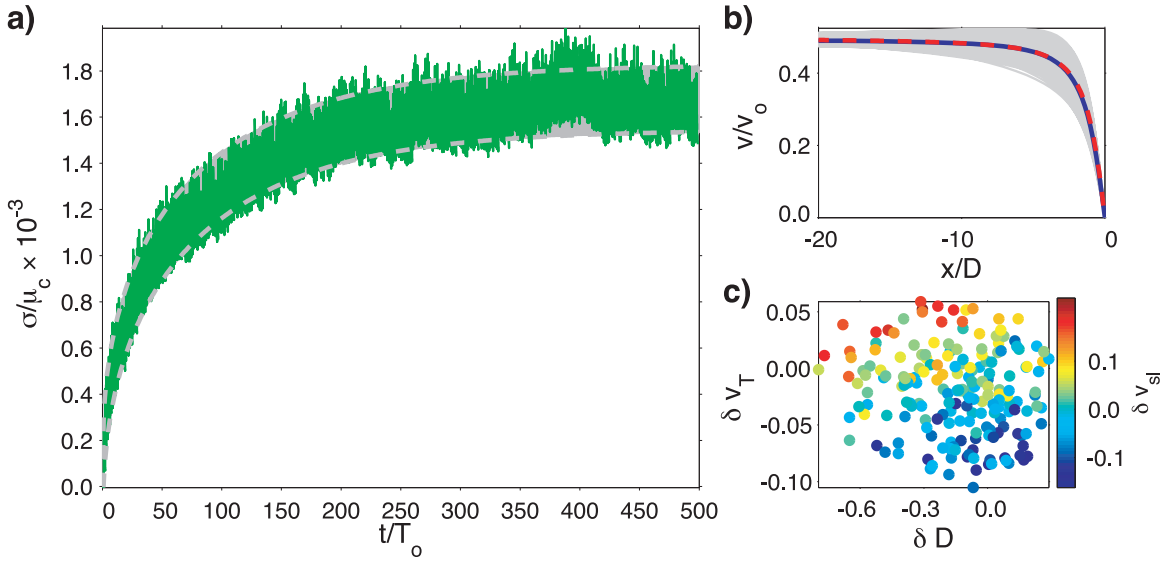

Figure 7. (a) Shear stress on a fault in a two-layer model with Maxwell rheologies ($\alpha_2/\alpha_1 = 1.3$, $\tau_{hs}/\tau_{ml} = 50$, and $\tau_o = T_o|\alpha_1| = 5$) and a random repeat time and rupture magnitude ($T = T_o \pm T_o/10$ and $\Delta = \Delta_o \pm \Delta_o/10$; green). Shear stresses for the same model but rupturing with constant repeat time T_o and rupture magnitude Δ_o are shown for reference (gray, limits shown as dashed gray lines). (b) Average interseismic velocities throughout the last 200 cycles (blue line) and the primary velocities (red dashed line). The average velocities in each cycle are shown to indicate the variation of velocities (gray lines). (c) Apparent locking depth (D) and velocity (v_T) in each of the last 200 cycles as a percent of the phase parameters of the primary velocities ($\delta X = (X_I - X)/X_I$, where X is D or v_T, and D_I and v_I are the parameters of the CEHM fit to the primary velocities); color scale denotes the average slip rate of the previous six cycles as a percent of $v_o = \Delta_o/T_o$.

the fault during spin-up does depend on T, since $\sigma_f/\mu_c \sim \frac{\Delta}{|\alpha_1|T}$. We take the rupture offset (Δ) divided by the time since the last rupture (T) to be the fault slip rate, and thus σ_f is proportional to the slip rate of the fault, $v_{sl} = \Delta/T$. During nonperiodic fault rupture sequences, the slip rate of the fault changes from cycle to cycle, hence σ_f is not constant during the rupture sequence.

2.6. Mature Deformation During a Random Rupture Sequence

[32] Just as the mature interseismic deformation is independent of the fault loading during periodic rupture sequences [e.g., *Li and Rice*, 1987; *Hetland and Hager*, 2004], when the rupture sequence is random, the interseismic velocities also do not depend on fault loading (see Appendix C). We can characterize whether the velocities in each cycle of a random rupture sequence are faster or slower than the primary velocities by the phase variables from a CEHM fit to the average interseismic velocities within each cycle (see section 2.3.1). Velocities faster than the primary velocities are fit by a CEHM with v_T larger than the actual, while slower velocities will be fit by a CEHM with a lower v_T. The interseismic velocities are generally larger than the primary velocities when the average slip rate over the past few seismic cycles has been faster than the long-term average (Figure 7c). Alternatively, when the slip rate has been consistently slower than the long term average over the past several cycles, the velocities are generally slower than the primary velocities. When the slip rate has varied rapidly over the past several cycles, the apparent v_T of the average velocities in each cycle varies from the average slip rate randomly (Figure 7c).

3. Strain Accumulation With Variable Fault Activity

[33] In section 2.6, we demonstrated that when the fault rupture sequence is not periodic, the interseismic stresses and velocities evolve from cycle to cycle in a fairly predictable manner. In this section, we clarify the variation of interseismic deformation with variations of fault rupture activity; however, instead of considering a random rupture sequence, we consider the simple cases of instantaneous changes in fault rupture magnitude and repeat time, both in unison with the fault loading rate and when the loading rate remains constant, separated by

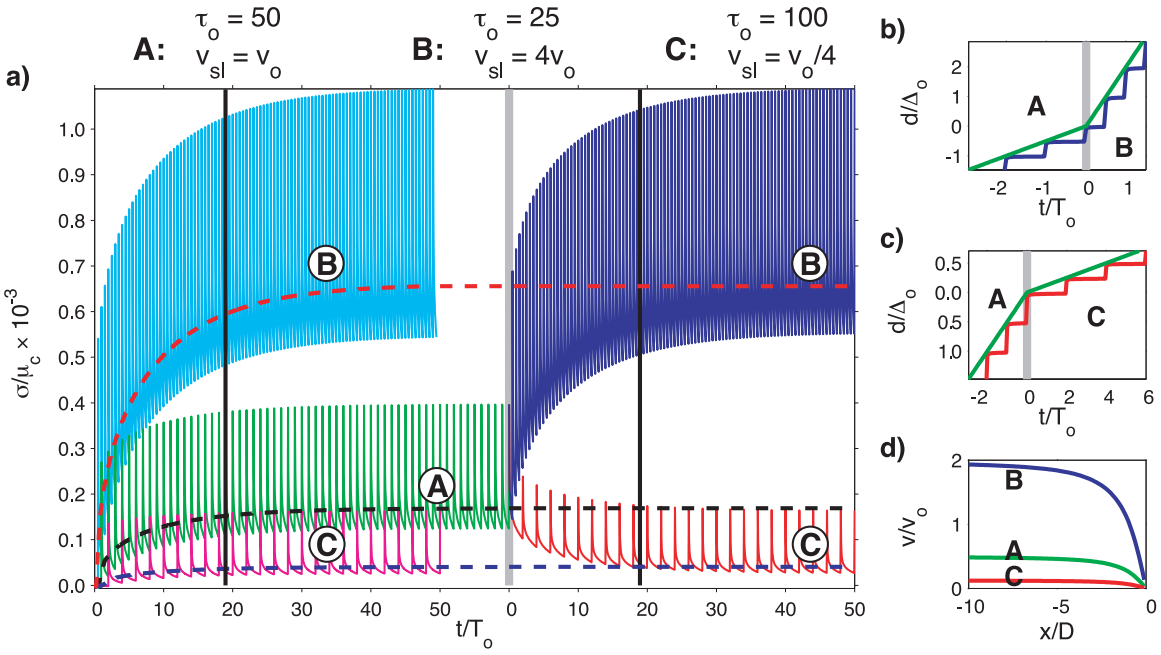

Figure 8. (a) Shear stress on a fault as a two-layer model with Maxwell rheologies ($\alpha_2/\alpha_1 = 1.35$ and $\tau_{hs}/\tau_{ml} = 50$) spins-up to a cycle invariant state, with $\tau_o = 50$ and slip rate v_o (green; state A), $\tau_o = 25$ and $4v_o$ (cyan; state B), and $\tau_o = 100$ and $v_o/4$ (magenta; state C). Also shown is the average shear stress through each cycle (dashed lines) and N_i (black solid lines). After the model with $\tau_o = 50$ (state A) reaches invariance, the slip rate of the fault and the boundary conditions are changed to $4v_o$ (blue; state B) or $v_o/4$ (red; state C). (b and c) Displacements at the fault and far-field for the transition from state A to B and from state A to C. (d) Primary velocities corresponding to the slip rates of states A, B, and C.

several rupture cycles. We only consider models with Maxwell viscoelastic rheologies where the fault is loaded purely by far-field shear.

3.1. Changes in Both Activity and Fault Loading

[34] When a fault with slip rate v_o is at cycle invariance, and both the slip rate of the fault and the far-field velocities change in unison, the shear stresses on the fault evolve to new cycle-invariant stresses. If σ_f is the change in stress during the initial spin-up, the stresses will change by $\sigma'_f - \sigma_f$, where σ'_f is the change in stress during the spin-up of a fault with the new slip rate and fault loading rate (Figure 8). The time that it takes to transition from σ_f to σ'_f is the same as the time it took to spin-up to the initial state (Figure 8). During this transition period the velocities vary from cycle to cycle, just as when the model spun up to its initial state. When the slip rate and the far-field velocities increase, the velocities are always larger than the initial cycle-invariant velocities, as the velocities build up to those that average to the new, larger primary velocities (Figure 8d). On the other hand, when the slip rate and far-field velocities decrease, the interseismic velocities decrease from cycle to cycle as the velocities change to the new lower, cycle-invariant velocities.

3.2. Changes in Fault Activity With Constant Fault Loading

[35] When the fault slip rate changes while the fault loading conditions are steady in time, the shear stresses on the fault will again deviate from the initial mature stresses. For instance, when the slip rate of a fault, initially slipping at v_o, decreases (i.e., longer repeat times and/or smaller ruptures), the stresses on the fault tend toward lower stresses corresponding to the new fault slip rate (Figure 9). However, since the far-field velocities do not change in unison with the fault slip rate, the model never reaches a new cycle invariant state (Figure 9). Instead the stresses near the fault continue to decrease from cycle to cycle due to the deficit in deformation near the fault compared to the far-field. Likewise, if the fault slip rate increases (i.e., shorter repeat times and/or larger ruptures), the stresses on the fault increase toward a new, higher

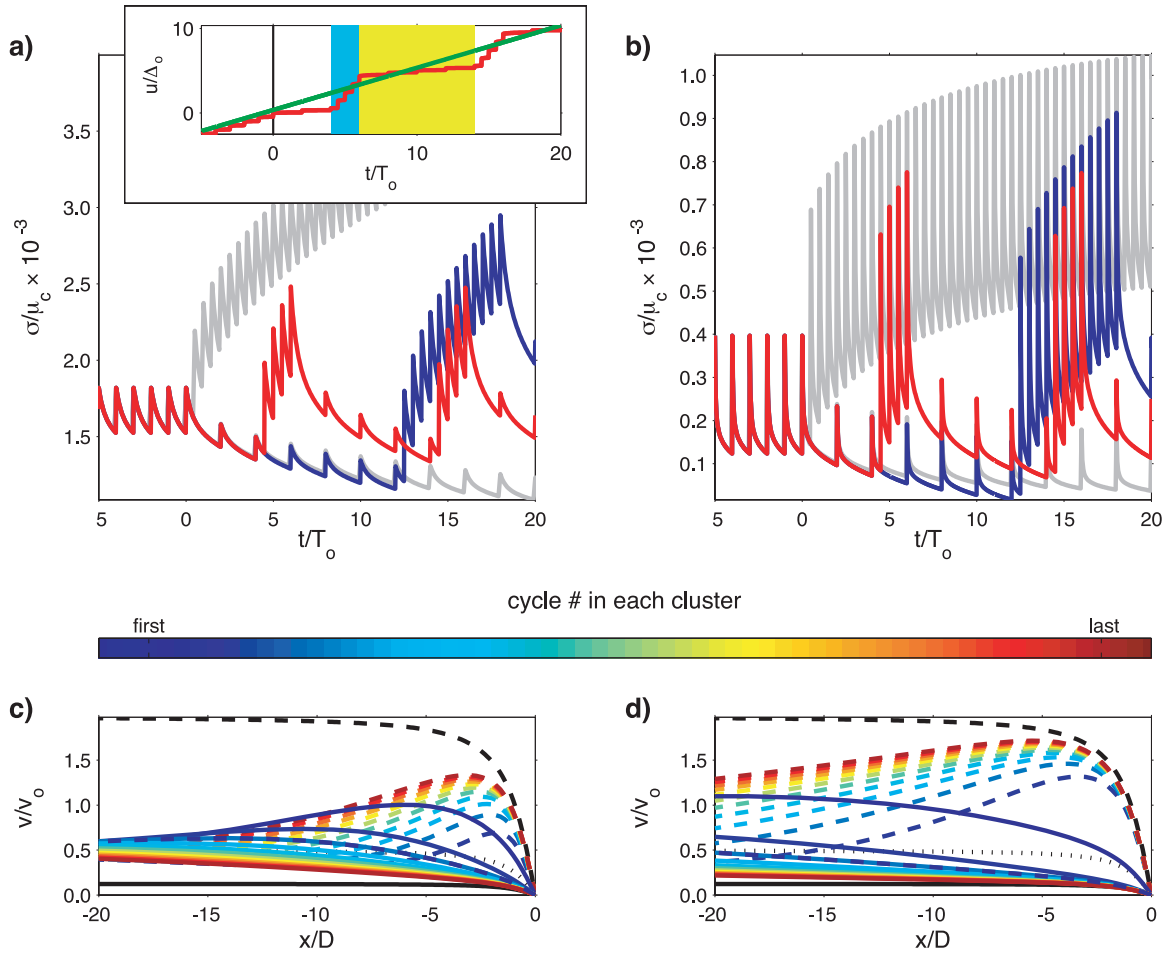

Figure 9. (a and b) Shear stresses on a fault in two-layer models with Maxwell rheologies (α_2/α_1 = 1.35 and τ_{hs}/τ_{ml} = 50) initially at a cycle invariant state, with $\tau_o = T_o|\alpha_1|$ = 5 (Figure 9a) and τ_o = 50 (Figure 9b), both with initial slip rate $v_{sl} = v_o$. At t = 0, the slip rate alternates between periods of $v_{sl} = v_o/4$ and $4v_o$ every fourth (red) or twelfth (blue) cycle, while the far-field velocities remain constant. Also shown is the shear stress on the fault for models where both the slip rate and the far-field velocities change from $v_{sl} = v_o$ to $v_o/4$ and $4v_o$ (gray; Figure 8). Inset of Figure 9a shows the displacements through time near the fault (red) and in the far-field (green) corresponding to the red stress history. (c and d) Average interseismic velocities during each of the 12 cycles of fast slip (dashed colored lines; cyan shaded region in inset) and slow slip (solid colored lines; yellow shaded region in inset) clusters for τ_o = 5 (Figure 9c) and τ_o = 50 (Figure 9d). Line color corresponds to the cycle within each cluster (blue through red is the first through last cycle), and the primary velocities for $v_{sl} = v_o/4$ (black solid line) and $4v_o$ (black dashed line) are shown for reference.

level, but since the far-field velocities are constant, the stresses continue to increase (Figure 9).

3.2.1. Constant Loading With Variable Fault Slip Rate

[36] To gain some insight into how the interseismic velocities vary after the fault slip rate changes, we consider the periods when v_{sl} is different than the far-field velocities as deviations from an initial cycle-invariant state with $\tau_o = T_o|\alpha_1|$ and $v_{sl} = v_o$, where T_o is the initial rupture repeat time and v_o is the difference in the far-field velocities across the fault. To keep the stresses from growing infinitely, we constrain the long term average slip rate to be v_o. During times when the fault slip rate is faster (slower) than v_o, the velocities are higher (lower) than the invariant velocities, as the shear stresses on the fault increase (decrease) (Figure 9). During periods of nonregular fault activity, the distance at which the velocities do not change from the initial invariant velocities is closer to the fault when τ_o is low compared to when τ_o is high (Figure 9).

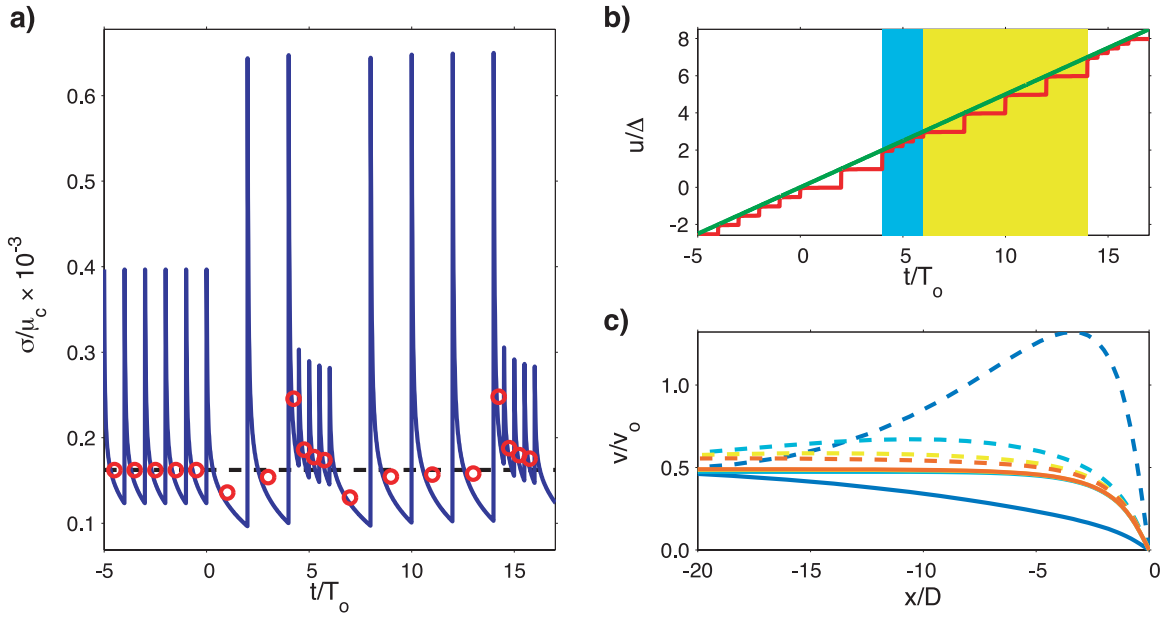

Figure 10. (a) Shear stress on a fault in a two-layer model with Maxwell rheologies ($\alpha_2/\alpha_1 = 1.35$ and $\tau_{hs}/\tau_{ml} = 50$) initially at cycle invariance, with $\tau_o = 50$ and slip rate $v_{sl} = v_o$. At $t = 0$ the magnitude and recurrence time of the ruptures alternates between clusters of large and small ruptures, with repeat times such that $v_{sl} = v_o$ at all times; red dots indicate the average shear stress in each cycle, and the black dashed line is the average mature stress for $v_{sl} = v_o$. (b) Displacements through time next to the fault (red) and in the far-field (green). (c) Average interseismic velocities during the small (dashed colored lines; cyan shaded region in inset) and large (solid colored lines; yellow shaded region in inset) rupture clusters; line color corresponds to the cycle within each cluster (blue through red are the first through last cycles).

3.2.2. Constant Loading and Fault Slip Rate

[37] If the repeat time and rupture magnitude temporarily change from T_o and Δ_o to aT_o and $a\Delta_o$, respectively, the slip rate remains constant. Since $\sigma_f \sim v_{sl}$, if the initial state is cycle-invariant, then the average mature shear stress on the fault will remain at the same level. However, when the rupture repeat time becomes longer than T_o, right after the last regularly repeating rupture the interseismic stresses continue to decrease past the lowest stress level during a periodic cycle, resulting in a lower average interseismic shear stress (Figure 10). On the other hand, if the new repeat time is shorter than T_o, the stresses do not decrease as much at the end of the cycle as the preseismic stress in a periodic rupture sequence, resulting in a higher average interseismic stress (Figure 10). In both cases, the system will respond so that the average interseismic shear stress on the fault evolves back to the mature, cycle-invariant level (Figure 10a). Additionally the velocities increase (decrease) from one cycle to the next during periods when the repeat time is longer (shorter) than T_o (Figure 10c).

4. Parallel Strike-Slip Faults

[38] In continents, rarely is deformation accommodated by a single fault, and almost always several faults are located within less than 10–20 locking depths (about 100–300 kilometers) from each other. In a model with linear rheologies and two strike-slip faults offset from each other (Figure 1e), the final mature shear stresses on each fault are not the same as if the faults had spun-up isolated from each other. Instead the shear stresses are the superposition of the stresses due to the spin-up of that fault and the spin-up of the offset fault. At a distance from the fault, the shear stress relative to the stress on the fault depends on the rheologies of the model. The stresses near the fault are larger in models with strong rheologies compared to models with weaker rheologies, while in the far-field they are smaller [e.g., *Lyzenga et al.*, 1991; *Roy and Royden*, 2000]. For example, in a model with strong rheologies, the stresses on a fault due to

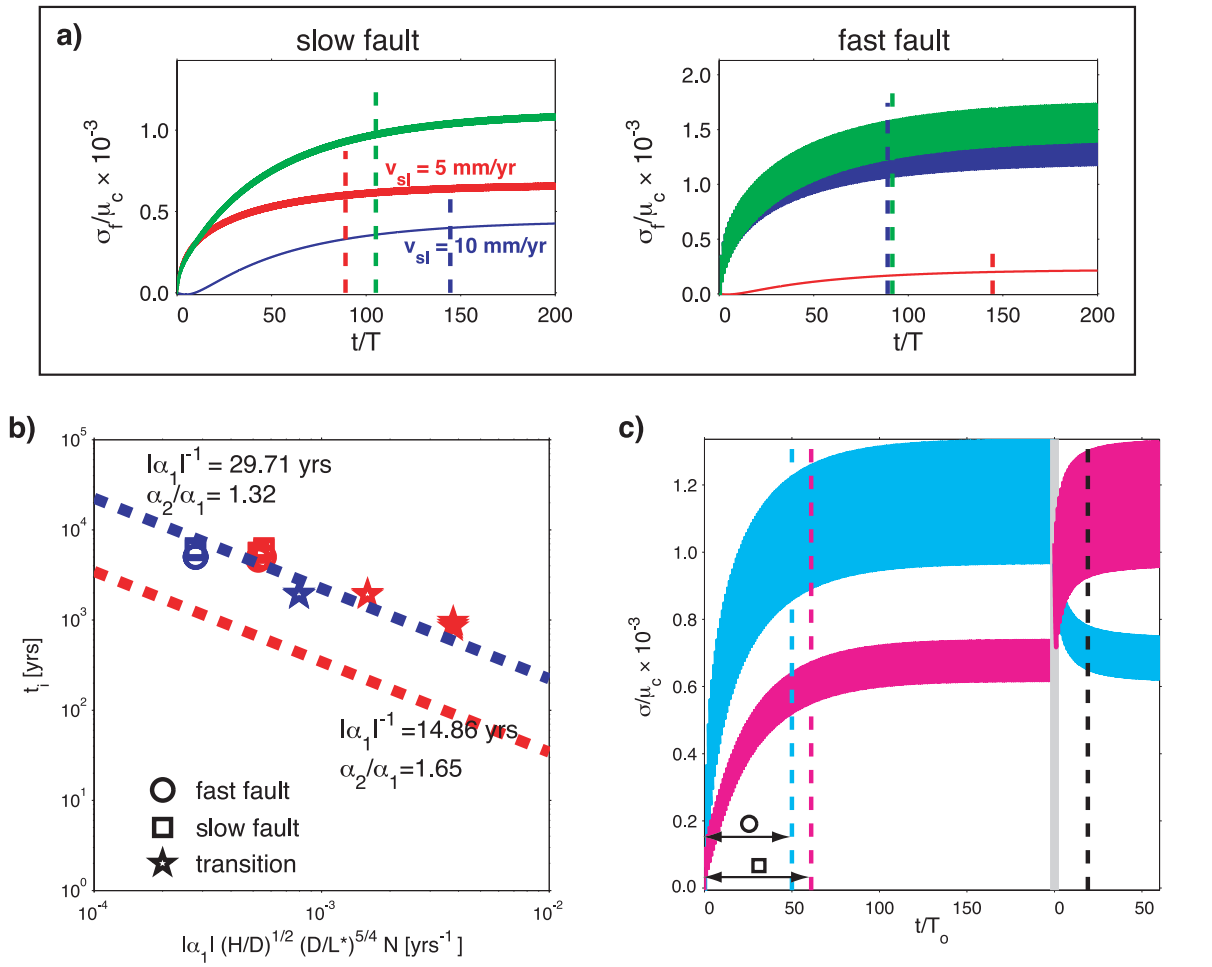

Figure 11. (a) Shear stresses on each fault during the spin-up of two faults in a two-layer model with Maxwell rheologies (α_2/α_1 = 2.2, τ_{hs}/τ_{ml} = 5, and τ_o = 3.4) and slip rates (v_{sl}) of 5 mm/yr (slow fault) and 10 mm/yr (fast fault), both with repeat time T_o, and separated by a distanced 20D. Shown are the stresses due to the slow (red) and fast (blue) faults, as well as the total stresses (green); N_i is marked for each stress history (dashed lines). (b) Spin-up times of each fault in two-layer models containing two faults separated by distance λ (circles and squares are the fastest and slowest slipping faults in each model), transition times (stars), and spin-up relations for a single fault in a two-layer model (dashed lines; Figure 6d). Blue symbols and lines correspond to α_2/α_1 = 1.32, and red corresponds to 1.65. N = 2 and $L^\star = L$ for the spin-up time, while N = 1 and $L^\star = \lambda$ for the transition. (c) Shear stresses on faults during the spin-up of a two-layer model with Maxwell rheologies (α_2/α_1 = 1.32 and τ_{hs}/τ_{ml} = 5) containing two faults, with slip rates of 15 mm/yr (cyan) and 5 mm/yr (magenta), separated by a distance of 20D. After the models spin-up to a cycle-invariant state, the slip rates on the faults instantaneously switch; N_i of each of the two faults (dashed lines, color corresponds to the stress history) and the transition period (black dashed line).

its own rupture history are larger than the stresses due to ruptures on the offset fault. Hence each fault is less affected by nearby faults when the rheologies are strong compared to models with weaker rheologies. Finally, since the interseismic stresses are proportional to the slip rate of the fault, a fast-slipping fault will generate larger stresses than a slower fault. For simplicity, we only consider periodic rupture sequences in this section; however, we do address a single instantaneous change in fault slip rate in section 4.2.

4.1. Spin-Up of Parallel Faults

[39] In a two-fault model, the deformation in the far-field is due to postseismic relaxation of both faults, and thus the velocities in the far-field build up to the mature, cycle-invariant velocities roughly twice as fast as in the one-fault models. When a

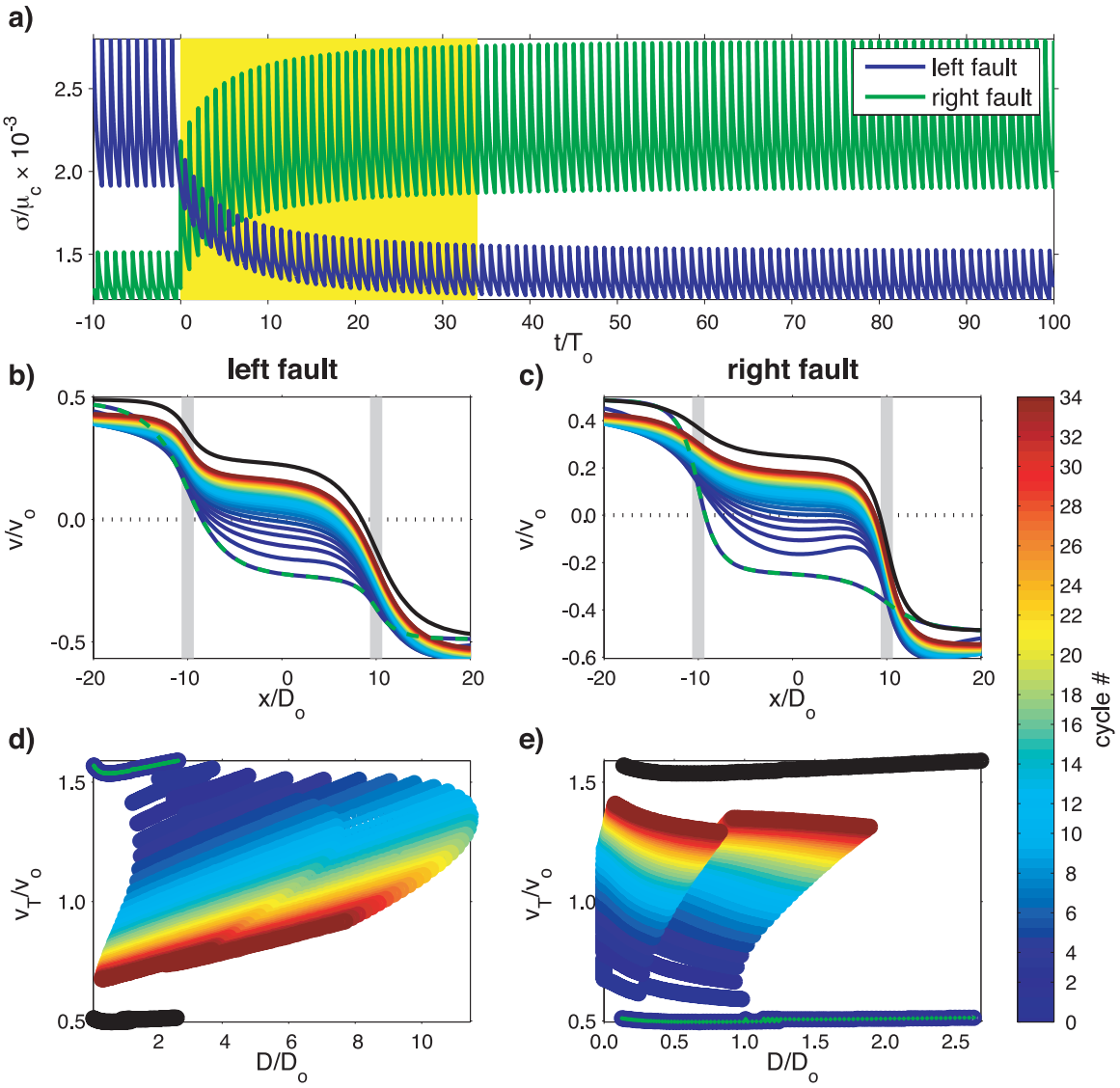

Figure 12. (a) Mature shear stresses on each fault in a two-fault, two-layer model with Maxwell rheologies (α_2/α_1 = 2.2, τ_{hs}/τ_{ml} = 5, and $\tau_o = T_o|\alpha|^{-1}$ = 3.4). Both faults initially rupture with repeat time T_o, and the rupture offset of the left and right faults is $3\Delta_o/2$ and $\Delta_o/2$, respectively, $T_o/2$ out of phase of each other, then at t = 0 the slip rates of the faults instantaneously switch. (b and c) Interseismic velocities immediately before each rupture on the left (Figure 12b) and right (Figure 12c) fault during part of the transition time highlighted in yellow in Figure 12a. Green dashed lines are the initial invariant velocities and black solid lines are the final invariant velocities. (d and e) Phase variables D and v_T of the left (Figure 12d) and right (Figure 12e) faults. Green dots and black circles indicate the phase variables during the initial and final invariant cycles, respectively.

fault is loaded by far-field shear, during the spin-up the velocities approach the invariant velocities near the fault faster than they do at a distance from the fault (Figure 3). Therefore the average stresses throughout each seismic cycle level off to a constant value at a slightly later time away from the fault compared to near the fault. In a two-fault model, where both faults are the same distance from the model boundaries (Figure 1e), each fault matures at different times if the slip rate of the two faults is different. When one fault has a much lower slip rate than the other, the stresses due to the slow fault on the fast fault are negligible, and the fast fault spins up as if the other fault were not there (Figure 11a). On the other hand, the stresses on the slow fault due to ruptures of the fast fault are comparable to the stresses due to the ruptures of the slow fault, and thus the slow fault becomes

invariant at a delayed time (Figure 11a). Additionally, when the rheologies are weak, the spin-up time of each of the faults is longer than in single fault models, whereas for stronger rheologies the spin-up times are not as lengthened since the faults are more rheologically isolated from each other (Figure 11b). In a multiple fault model, the spin-up depends on all of the model parameters (e.g., the slip rates, distance between faults, rheologies). It is not our intention to determine the relationships of the spin-up time and the final average shear stresses to the model parameters in multifault models; however, the variations from the single fault models can be understood through the above illustrations.

4.2. Repartitioning of Slip Rates on Parallel Faults

[40] As in the single-fault examples in section 3.2, when the slip rates of each fault in a two-fault model change, the stresses on the faults evolve toward new cycle-invariant levels. Unlike the single-fault examples, there is no deficit or excess deformation between the far-field and near the fault when the far-field velocities remain constant as long as the sum of the slip rates of the faults remains constant; hence the fault system will reequilibrate to a new mature, cycle-invariant state after the fault slip rates change (Figure 11c). The time to transition to the new state is roughly given by the relations in section 2.4, using the fault offset distance as the model's length scale instead of the distance to the model boundaries (Figure 11b). The smaller model length scale reflects that the deformation only changes in the near field, and when the total slip rate is conserved, stresses are only transferred over the distance between the faults. Thus the time to transition to the new mature state is much less than the time that it took for the faults to initially reach cycle invariance. As in the initial spin-up time, when the rheologies are extremely weak, the system reequilibrates over very few cycles, whereas when the rheologies are strong, the transition period lasts many cycles. Finally, the time to reequilibrate is sometimes delayed due to the effects of the faults on each other, as explained in section 4.1.

[41] After the slip rates change, the interseismic velocities during the transition period are those required to increase or decrease to the new cycle-invariant velocities (Figure 12). The interseismic velocities near the fault whose slip rate has decreased are consistently slower than during the initial cycles, and its apparent locking depth throughout each cycle is consistently larger than during the initial cycles (Figure 12d). Alternatively, the interseismic velocities near the fault whose slip rate has increased are larger than the initial velocities as the new, larger cycle-invariant velocities are built up, and the apparent locking depth throughout each cycle is smaller than it was before the slip rate change (Figure 12e). Additionally, the phase variables of the fault that has slowed down (sped up) vary within each cycle more (less) than in the initial invariant cycles (Figure 12). Finally, the apparent slip rate of the faults varies rapidly from cycle to cycle immediately after the slip rates change, and approaches the new invariant state more slowly later in the transition period (Figure 12).

5. Discussion

[42] Throughout this paper, we have focused on models with relatively simple geometries and Maxwell viscoelastic rheologies, and in the following subsection, we discuss the effects of including more complex rheologies. In section 5.2, we discuss the results we have reported in the context of strain accumulation models. As we have also imposed fault activity, in section 5.3, we discuss the stability of periodicity in fault ruptures and the connection to these results. Finally, in section 5.4, we discuss the implications of the previous sections to geodetic studies in southern California.

5.1. Model Rheologies

[43] In addition to the above-two dimensional models of linear Maxwell rheologies, the spin-up to a mature state is characteristic of models with general viscoelastic rheologies [*Hetland and Hager*, 2005] and nonlinear rheologies [*Lyzenga et al.*, 1991], and models accommodating postseismic afterslip [*Johnson and Segall*, 2004], as well as three-dimensional models [e.g., *Lynch et al.*, 2003]. When the lower half-space of a one layer model has a Burgers viscoelastic rheology, the cycle-invariant interseismic velocities differ from those predicted by a model with only Maxwell rheologies [*Hetland and Hager*, 2005]. Likewise, the interseismic velocities throughout seismic cycles of nonperiodic rupture sequences differ. However, as the spin-up time is dominated by the nonrecoverable, steady relaxation, the evolution of the shear stresses from cycle to cycle is approximately the same in the Burgers model as in the Maxwell model.

[44] In general, the spin-up of a model is dominated by the slowest recoverable phase of the rheology. In a mature system, when the fault slip rate differs from the long-term average, the rate of evolution of interseismic deformation will be affected by the presence of other, weaker relaxation phases; however, the trend of the evolution will be the same as for these univiscous examples. For example, in a model with multiviscous rheologies, near a fault whose slip rate has been faster than the long term average, interseismic velocities will be larger than the cycle-invariant velocities.

5.2. Models of Strain Accumulation

[45] When a fault ruptures repeatedly, the fault will always evolve toward a mature state. In a mature state, the interseismic velocities throughout the seismic cycle are perturbations to the primary velocities, which are the average interseismic velocities in addition to the velocities of the equivalent elastic model. The perturbations through time are determined largely by the rheologies of the model. Solutions for interseismic deformation are known for models with Maxwell rheologies [e.g., *Savage and Prescott*, 1978; *Savage*, 2000; *Pollitz*, 2001; *Smith and Sandwell*, 2004], Maxwell rheologies with viscous fault slip [*Johnson and Segall*, 2004], and general linear viscoelastic rheologies [*Hetland and Hager*, 2005]; however, interseismic deformation has not been determined for more complex rheologies. Models with segmented faults with different rupture histories, either segmented in depth or along strike, will likewise evolve toward a mature state; however, the interseismic deformation in segmented fault models is spatially and temporally complex.

[46] On established faults, the entire interseismic period is part of one process, resulting from the cumulative effect of all previous ruptures, on all faults in the region [e.g., *Bott and Dean*, 1973; *Savage and Prescott*, 1978; *Pollitz*, 2003a]. In general, during the interseismic period there is no natural division between postseismic and relaxed periods. Naturally, there may be times early in the seismic cycle when the deformation is dominated by transient postseismic processes, whereas later in the cycle the deformation is relatively steady. Nevertheless, just as the postseismic deformation depends on the secular fault reloading [e.g., *Montèsi*, 2004], the deformation late in the cycle depends on the early transients, and cannot be considered independent of all the rheological processes.

[47] Researchers sometimes assume that deformation before large strike-slip earthquakes is that of simple shear [e.g., *Vergnolle et al.*, 2003; *Freed and Bürgmann*, 2004; *Pollitz and Nyst*, 2005], and most researchers model postseismic deformation ignoring all but the last earthquake [e.g., *Hearn et al.*, 2002; *Hetland and Hager*, 2003; *Pollitz*, 2003b]. Only when all of the relaxation times of the model are much shorter than the rupture repeat times is the deformation late in the cycle close to that of simple shear, and can the postseismic deformation be considered independently of all previous ruptures. This corresponds to large τ_o in a one-layer model, with only one viscous phase [*Savage and Prescott*, 1978]. However, as mentioned before, when the transient deformation from the most recent rupture varies much faster than the cumulative postseismic effects of all but the last rupture, the interseismic velocities observed immediately before the last rupture can approximate the cumulative effects of the previous ruptures throughout the postseismic period [e.g., *Bürgmann et al.*, 2002; *Hearn et al.*, 2002].

[48] In a layered model with or without multiviscous rheologies, all of the relaxation times need to be small compared to the rupture repeat times for the deformation late in the cycle to be simple shear. The cycle-invariant velocities in a model with strong rheologies are similar to those of simple shear plus the postseismic velocities from a single rupture in a Maxwell model with a short relaxation timescale (Figure 13). In order to obtain an accurate understanding of the rheology, the strain accumulation from the entire rupture history needs to be considered.

[49] For example, models of the postseismic deformation from the 1992 Landers and 1999 Hector Mine earthquakes by *Pollitz et al.* [2001] and *Freed and Bürgmann* [2004] have assumed Maxwell rheologies, attributing the rapid postseismic deformation observed to a low effective viscosity of the Maxwell dashpot. However, relatively rapid interseismic strain rates were observed before the 1992 Landers earthquake [e.g., *Sauber et al.*, 1994], observations difficult to reconcile with a low Maxwell viscosity. It seems more likely that the postseismic transient was the result of a transient rheology [e.g., *Pollitz*, 2003b], although a quantitative analysis employing a Burgers rheology to model both the interseismic deformation observed before the ruptures and the postseismic deformation is beyond the scope of this paper. *Vergnolle et al.* [2003] interpreted geodetic mea-

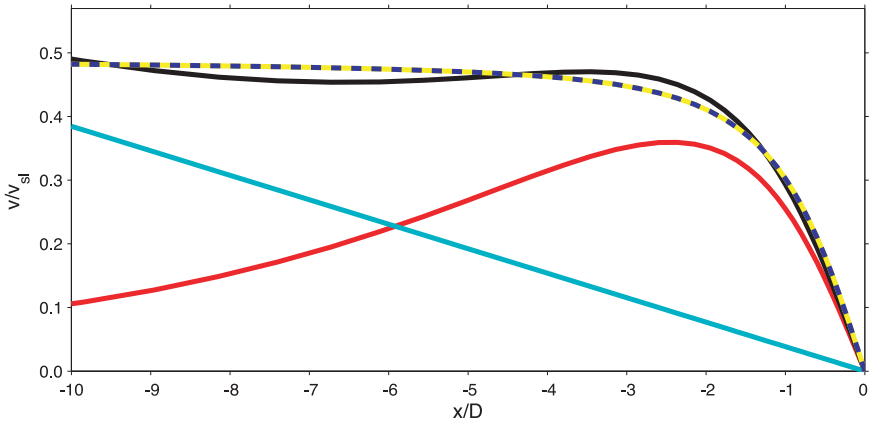

Figure 13. Velocities (black) of a model composed of the postseismic velocities after a single rupture (red) plus those of distributed shear (cyan), and the interseismic velocities for a classic elastic half-space model (blue-yellow dashed line).

surements of interseismic velocities across several faults in Mongolia as due to the cumulative effects of rigid rotation, 3–5 mm/yr of simple shear, and postseismic transients from four large ruptures in the last 100 years. They inferred mantle and lower crust viscosities of about 10^{18} and 10^{17} Pa·sec. However, since their maximum interseismic contribution to the geodetic velocities is about 2 mm/yr, and depending on the fault activity prior to the most recent earthquakes, it may be possible that a strain accumulation model with stiffer rheologies, with interseismic deformation nearly that of the CEHM, may be able to explain the data as well. As before, a quantitative study of this region is beyond the scope of the this paper.

5.3. Stability of Nonperiodic Rupture Sequences

[50] In all of these examples, we have prescribed fault ruptures. In reality, a fault ruptures when shear stresses exceed the frictional strength of the fault [e.g., *Scholz*, 1998]. In our fault rupture models, shear stresses decrease during the interseismic period and increase during the rupture. If the fault rupture were governed by friction, the variations in stress would be expected to be the opposite. However, the stress histories shown here can be converted to the frictional fault case by prestressing the model. For example, in a model loaded by far-field shear, sufficient initial stresses are developed by shearing the model for a period of time before the first rupture (Figure 4b). Assuming that the fault was initially loaded in this way, when a regularly scheduled rupture in a periodic rupture sequence is missed (i.e., the repeat time becomes longer), the stresses on the fault continue to increase past the stress level before the last rupture. Alternatively, in the case when the fault ruptures before a regularly scheduled rupture, the stresses on the fault do not reach the same preseismic stress level (e.g., Figures 9 and 10). Hence several researchers who have proposed models of nonperiodic rupture sequences have appealed to nonsteady friction [e.g., *Chèry et al.*, 2001; *Kenner and Simons*, 2005].

[51] Using a one dimensional slider-block model with a Maxwell viscoelastic rheology, *Kenner and Simons* [2005] deduced a nondimensional number that typifies the tendency of faults to rupture periodically or nonperiodically. They called this number the Wallace number, after Robert E. Wallace, who first documented clustering in the western US [*Wallace*, 1987]. The Wallace number, W, is defined as the ratio of the stress drop in an earthquake to the reloading stress, and is equivalent to $2T_o/\tau_M$, where T_o is the average rupture repeat time and τ_M is the effective Maxwell relaxation time [*Kenner and Simons*, 2005]. For W less than about one, *Kenner and Simons* [2005] showed that periodic fault activity is stable. As W increases, rupturing exhibits increasing nonperiodic behavior, and when $W > 100$ the fault ruptures tend to cluster in time.

[52] In two-dimensional, linear viscoelastic models of infinite length frictional faults, the tendency toward nonperiodic rupture sequences is similar to that of the slider-block models [*DiCaprio et al.*, 2004]. In three-dimensional, linear viscoelastic models with frictional faults, T_o/τ_M is also the parameter that controls the tendency of faults to

rupture nonregularly [*Lynch et al.*, 2003; *Chèry et al.*, 2001], while a difference in strengths of nearby faults appears to be required for ruptures to cluster in time [*Lynch et al.*, 2003]. The relationships of W to all of the model parameters in two and three-dimensional models have yet to be published.

[53] We speculate that in viscoelastic models, the Wallace number is proportional to $T_o|\alpha_1|$. In the two-dimensional viscoelastic models considered in this paper, W also must depend on the geometry and rheology terms in the relations given in section 2.4. For the standard model of *Savage and Prescott* [1978], $|\alpha_1| = 1/2\tau_M$, and, ignoring the possible dependence on other model parameters, $W = 4\tau_o$. Assuming that the fault is initially unstressed, after the fault spins up to a mature state, the long-term average shear stress on the fault is σ_f. If the fault slip rate changes, the stresses on the fault evolve toward a new average, σ'_f. Assuming that the stress drop in a rupture (σ_{eq}) is proportional to $\mu_c\Delta/D$ [e.g., *Lay and Wallace*, 1995], $\partial\sigma/\partial\sigma_{eq} = \Lambda\tau_o^{-1}$, where $\partial\sigma = \sigma_f - \sigma'_f$, $\partial\sigma_{eq} = \bar{\sigma}_{eq} - \sigma'_{eq}$, $\bar{\sigma}_{eq}$ is the long-term average σ_{eq}, and Λ includes the dependence on the model rheologies and geometries. When τ_o is small, $\partial\sigma \gg \partial\sigma_{eq}$ and the deviations from a periodic rupture sequence produce large stresses. Unless these stresses are absorbed elsewhere in the model or the fault strength varies widely, such deviations from periodicity are not stable. Alternatively, when τ_o is large, $\partial\sigma \ll \partial\sigma_{eq}$ and deviations from periodicity produce negligible stresses, and thus nonperiodic rupture sequences are relatively stable. In the case when the fault slip rate alternates between periods with $v_{sl} \ll v_o$ and $v_{sl} \gg v_o$, where v_o is the long term slip rate of the fault, the change in stress on the fault during periods of heightened activity is large because $\partial\sigma_{eq}$ is large, hence such extremely dense clusters may not be stable except for extremely weak rheologies.

5.4. Applications to Geodetic Studies

[54] The success of a block model to describe observed interseismic deformation in southern California, led *Meade and Hager* [2005a] to suggest that $\tau_o < 0.5$ and the viscosity of the aseismic lithosphere is greater than about 10^{19} Pa·sec. Studies of postseismic deformation following large earthquakes in this region have suggested lower viscosities [e.g., *Pollitz et al.*, 2001]; however, these rapid transients may not reflect the steady viscosity of the lithosphere [e.g., *Ivins*, 1996; *Pollitz*, 2003b; *Freed and Bürgmann*, 2004]. *Meade and Hager* [2005a] did not use data affected by the postseismic response of these earthquakes, and thus their results are not directly sensitive to any rapid rheological phases. The lower viscosity bound obtained by *Meade and Hager* [2005a] was based on the relationship between τ_o and viscosity from the standard interseismic model of *Savage and Prescott* [1978]. Using a one-layer model of interseismic deformation with both Maxwell relaxation and viscous fault slip, *Johnson and Segall* [2004] estimated that the steady viscosity under California is 10^{19}–10^{20} Pa·sec. The use of layered viscoelastic models will affect the bounds on the rheology [e.g., *Savage*, 2000]; however, *Fay and Humphreys* [2005] inferred a similar viscosity bound using a layered model, and thus the conclusion that $\tau_o < 0.5$ for the deformation to not vary through most of the seismic cycle is largely independent of the particular model geometry.

[55] In southern California, almost all active faults appear to rupture irregularly [e.g., *Grant and Sieh*, 1994; *Weldon et al.*, 2004]. Using the upper bound on τ_o of *Meade and Hager* [2005a] and assuming that τ_o maps to the Wallace number four to one, in southern California $W < 2$, indicating that nonregular ruptures may be at most slightly stable, so deviations from periodic rupture sequences will lead to the buildup of large residual stresses. Three dimensional effects may produce a situation in which irregular rupturing was more favored; however, *Chèry et al.* [2001], albeit using simple three-dimensional geometries, showed that faults exhibit no clustering of ruptures with $\tau_0 \approx 3$. If the ranges of W for clustering to be stable in three dimensional models is the same as that for one-dimensional models, the mapping from τ_o to W would need to increase by an order of magnitude or more for nonperiodic fault activity to be stable in southern California.

[56] Inherent in block models is the assumption that all of the faults are mature and that interseismic velocities are everywhere those of an elastic model (i.e., the primary velocities). Several researchers have suggested that fault systems in southern California are undergoing relatively rapid redistribution of slip rates [e.g., *Sharp*, 1981; *Peltzer et al.*, 2001]. For example, paleoseismic evidence indicates that the slip rate of the San Jacinto (SJ) fault has increased over the Holocene [*Sharp*, 1981], while geodetic estimates of the slip rate of the adjacent San Bernadino segment of the

San Andreas (SA) are lower than the Holocene rates [e.g., *Meade and Hager*, 2005a]. Assuming that the SJ-SA fault system was at a mature state before the slip rates changed, a model of two faults offset a few locking depths from each other should take up to about 50 seismic cycles to reequilibrate to a new mature state. If the slip rates of the faults have varied within the past tens of seismic cycles, the present interseismic velocities are not the primary velocities, and the fault parameters estimated in the block model are biased. The mapping of the estimated variables to the actual fault locking depths and slip rates would require three-dimensional fault geometries to be considered, and is beyond the scope of this paper.

[57] The initial question of the time it would take the San Andreas fault system in southern California to mature can also be considered. Ignoring three-dimensional effects and the effects of faults on each other, and assuming $\tau_o = 0.5$, we can use the relations in section 2.4 to begin to address the issue. For a fault rupturing through an elastic layer over a viscoelastic half-space, it would take on the order of tens of cycles to reach a mature state when the fault is loaded by steady sliding on the extension of the fault at depth. Assuming the other end-member fault loading mechanism of far-field shear, for the same rheology it would take about 20–60 cycles if the far-field shear is applied 1000 km from the fault ($D/L \approx 66.67$). As the distance from the fault to the constant shear conditions decreases (increases), the spin-up time is slightly shorter (longer), but not by more than a factor of 2–4 (Figure 6a). Instead of the one-layer geometry, we can also consider an elastic upper crust separated from a viscoelastic mantle by a viscoelastic lower crust (a two-layer model), with the fault loaded by far-field shear applied 1000 km from the fault. If the mantle is weaker than the lower crust, it might take up to about 100 cycles to approach a mature state, while if the mantle is much stronger than the lower crust, we would predict that it to take on the order of 100–200 cycles for the San Andreas to mature. Using a range of repeat times of 100–250 years on the San Andreas fault in southern California [e.g., *Weldon and Sieh*, 1985], 10–200 cycles corresponds to 1000–50,000 years.

[58] The fact that, except near recent large earthquakes, observed interseismic velocities do not vary with time over the past several decades, suggests that the inelastic rheology of the continental lithosphere is dominated by a relatively stiff viscosity [e.g., *Johnson and Segall*, 2004; *Fay and Humphreys*, 2005; *Meade and Hager*, 2005a]. Models with nonlinear or multiviscous rheologies, with weak viscous phases capable of explaining postseismic transient deformation, as well as a steady viscous phase with a time scale much longer than rupture repeat times, may be necessary to describe the deformation of the continental lithosphere over seismic cycle timescales [e.g., *Ivins*, 1996; *Pollitz*, 2003b; *Freed and Bürgmann*, 2004; *Hetland and Hager*, 2005]. With such multiviscous rheologies, interseismic velocities will vary little throughout most of the later seismic cycle, resembling those of a CEHM [*Hetland and Hager*, 2005]; however, these relatively steady interseismic velocities are still not the primary velocities. With such a multiviscous rheology, interseismic velocities still vary from the invariant velocities during nonperiodic rupture sequences [*Hetland and Hager*, 2005]. The stability of nonregular ruptures with multiviscous rheologies is potentially very important for an understanding of continental deformation.

6. Conclusions

[59] In this paper, we examined models of interseismic deformation near infinite-length strike-slip faults during the spin-up to a mature state, as well as during nonperiodic fault rupture sequences. We used models of an elastic layer over a linear viscoelastic half-space and an elastic layer over a viscoelastic middle layer and half-space. We concentrated on the univiscous Maxwell rheology, although we also used a biviscous Burgers viscoelastic rheology. We used two primary fault loading models: a fault driven by steady sliding of the down-dip extension of the fault [e.g., *Savage and Burford*, 1973; *Savage and Prescott*, 1978; *Hetland and Hager*, 2005], and a fault loaded by far-field shear boundary conditions [e.g., *Bonafede et al.*, 1986; *Lyzenga et al.*, 1991; *Pollitz*, 2001].

[60] During the spin-up, the stresses and velocities evolve from the initial to the mature. Over enough cycles such that the cumulative deformation is block-like, the mature shear stresses average to a level determined by the fault slip rate, the model rheologies, the fault loading conditions, and the initial stresses. However, for linear rheologies, the change in shear stress during spin-up is independent of the initial stresses. The initial velocities are determined by the fault loading model, while over a time window for block-like deformation, the average mature interseismic velocities equal the interseismic velocities of the equivalent elastic

model, also referred to as the primary velocities. During a periodic rupture sequence, the cumulative deformation is block-like at the end of one seismic cycle, and thus the average interseismic velocities equal the primary velocities over one seismic cycle. When the elastic shear modulus of the model is uniform, the equivalent elastic model is the classic elastic half-space model of *Savage and Burford* [1973]. The time that a fault model takes to reach a mature state depends on the fault loading conditions, the presence of other faults, and the rheology, but is largely dominated by the nonrecoverable viscous phase.

[61] Once the fault model spins-up, the deformation does not depend on the fault loading conditions, as long as the loading rate is constant in time [e.g., *Li and Rice*, 1987; *Zatman*, 2000; *Hetland and Hager*, 2004, 2005]. When the fault ruptures periodically, the mature interseismic deformation is cycle invariant (i.e., the same in all cycles) [e.g., *Savage and Prescott*, 1978]. When the fault ruptures nonperiodically, the fault spins-up to a mature state that is the same as if the fault had ruptured periodically with the mean repeat time and mean rupture offset. When the rupture sequence deviates from periodicity, the shear stresses on the fault and the interseismic velocities evolve toward the mature stresses and velocities given for the current slip rate. Around a fault whose slip rate is faster than average, interseismic velocities are larger than the invariant velocities and increase from cycle to cycle [see also *Meade and Hager*, 2004]. Alternatively, near a fault slipping more slowly than average, the velocities are lower than the invariant, and decrease from cycle to cycle.

[62] Except in a few rheological cases, heightened strain rates across faults are a consequence of repeated earthquakes within the region [e.g., *Bott and Dean*, 1973; *Savage and Prescott*, 1978; *Pollitz*, 2003a]. Only when the relaxation timescales of the lithosphere are much shorter than the rupture repeat times, is simple shear the correct preseismic deformation model and can postseismic velocities be considered independent of all previous earthquakes [e.g., *Savage and Prescott*, 1978]. When the relaxation times scales are much longer than the repeat times, the cycle-invariant velocities are those of the equivalent elastic model at all times during the seismic cycle [e.g., *Savage and Prescott*, 1978]. During the fault spin-up, periods of nonperiodic fault ruptures, and when slip rates repartition on adjacent faults, the interseismic velocities are not cycle-invariant. Whenever the velocities are not cycle-invariant, the average interseismic velocities over one seismic cycle are not the primary velocities. Researcher must consider the entire rupture history in order to get accurate assessments of model parameters, whether using dynamic models of postseismic relaxation or kinematic block models.

Appendix A: Finite Element Model Description

[63] We compute the deformation resulting from repeated earthquakes in two-dimensional models driven by far-field shear using the finite element program GeoFEST 4.5 [*Lyzenga et al.*, 2000]. The models are composed of strike-slip faults breaking an elastic upper layer overlying viscoelastic middle and lower layers. The viscosities and shear moduli of the middle and lower layers are either identical (a one-layer model) or distinct (a two-layer model). The two-dimensionality of the model implies that the fault is infinite in length. The fault uniformly breaks the upper elastic layer, and the fault offset tapers linearly to zero over one element in the lower viscoelastic region. The thickness of the upper layer and middle layer is D and H, respectively. We vary both D and H, and the nominal thickness of the upper layer is D_o. The distance from the fault to the sides of the models is variable, while we use a constant model thickness of $120D_o$.

[64] We use a graded element mesh, such that the node spacing is $0.2D_o$ over the upper and middle layers near the fault, and the node spacing increases by a factor of 1.2 toward the edges of the model. In depth, the mesh grading begins at the bottom of the middle layer, while laterally grading begins $2D$ from the fault. When there are two faults in the model, the node spacing is constant between the faults. We construct all of our models such that the upper and middle layers are resolved by at least two elements each; however, we only use these low resolution models in some calculations in section 2.4, while in other models we ensure that the upper two layers are each resolved by at least five elements. When the upper layer is resolved by five elements, the thickness of the layer is D_o.

[65] When the model contains one fault the deformation is antisymmetric, and we only model one half of the model, specifying a zero velocity boundary condition on the edge of the model containing the fault. When the model contains two faults, we compute the deformation in the entire model, and apply velocity boundary condi-

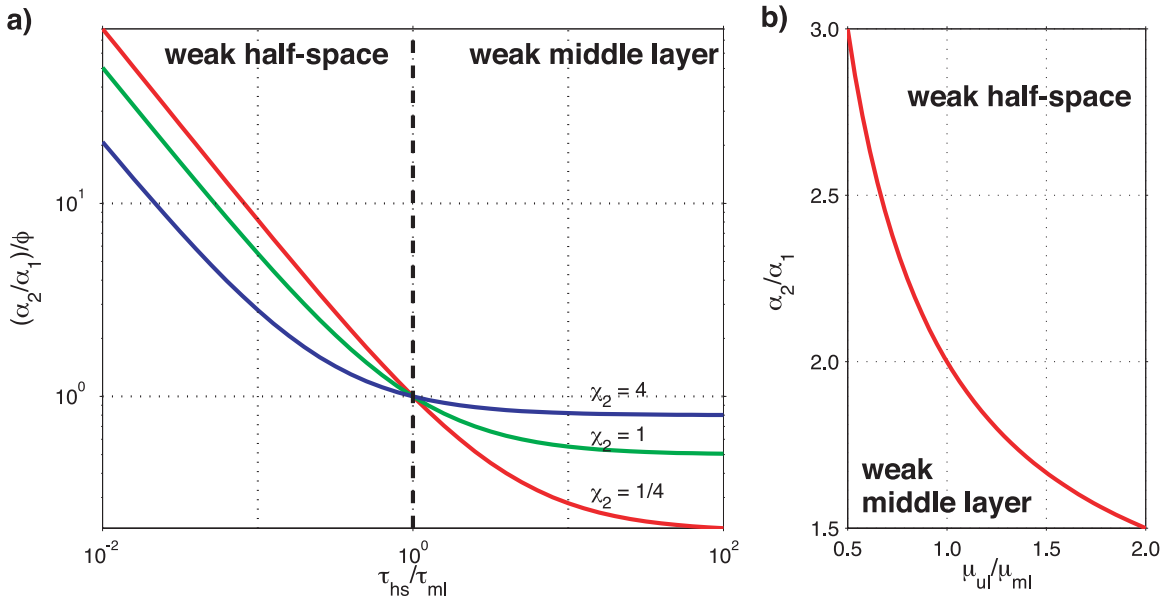

Figure B1. (a) Ratio of the coupling coefficients between the upper and middle layers (α_1) and the middle layer and lower half-space (α_2) normalized by $\phi = (\mu_{ul} + \mu_{ml})/\mu_{ul}$ as a function of τ_{hs}/τ_{ml}. Black dashed line is $\tau_{hs} = \tau_{ml}$. (b) α_2/α_1 for $\tau_{hs}/\tau_{ml} = 1$ as a function of μ_{ul}/μ_{ml}.

tions on both sides of the model. In all models, we apply constant velocity boundary conditions on the sides not containing faults, while the top and bottom of the model are free-slip.

Appendix B: Coupling Coefficients in Two-Layer Models

[66] In two-dimensional models of an elastic layer over a Maxwell viscoelastic middle layer and a Maxwell viscoelastic lower half-space, there are two timescales in the solution for the surface displacements due to coseismic stress relaxation [e.g., *Piersanti et al.*, 1995; *Hetland and Hager*, 2006]. In the two-dimensional models in this paper, these two timescales arise from the two mechanical coupling coefficients in the elastic image solution of *Chinnery and Jovanovich* [1972; *Hetland and Hager*, 2006]. Defining the subscripts "ul," "ml," and "hs" to signify the rheological parameters of the upper layer, middle layer, and lower half-space, the coupling coefficients are

$$\alpha_1 = -\frac{\chi_1}{(1+\chi_1)}\frac{1}{\tau_{ml}} \tag{B1}$$

and

$$\alpha_2 = -\frac{1+\chi_2\xi}{(1+\chi_2)\xi}\frac{1}{\tau_{ml}}, \tag{B2}$$

where $\chi_1 = \mu_{ul}/\mu_{ml}$, $\chi_2 = \mu_{hs}/\mu_{ml}$, $\xi = \tau_{hs}/\tau_{ml}$ and $\tau_x = \eta_x/\mu_x$ [*Hetland and Hager*, 2006]. The ratio of the coupling coefficients is

$$\frac{\alpha_2}{\alpha_1} = \frac{1+\chi_1}{\chi_1}\frac{1+\chi_2\xi}{(1+\chi_2)\xi}. \tag{B3}$$

When the middle layer is weaker than the lower half-space, $\tau_{hs} > \tau_{ml}$ and $\alpha_2/\alpha_1 < \phi$, where $\phi = (\mu_{ul} + \mu_{ml})/\mu_{ul}$ (Figure B1). For instance, when $\mu_{ul} = \mu_{ml}$, $\alpha_2/\alpha_1 < 2$ corresponds to a weak middle layer.

Appendix C: Dependence of Interseismic Velocities on Fault Loading

[67] Once the fault model spins-up with periodic ruptures, the cycle invariant velocities at the surface do not depend on the fault loading conditions, as long as the loading rate is constant in time [e.g., *Li and Rice*, 1987; *Zatman*, 2000; *Hetland and Hager*, 2004]. *Hetland and Hager* [2005] further noted that for a model that has spun-up to a mature state with a rupture sequence containing periodicity, the interseismic surface velocities predicted by a model where the fault is loaded by sliding on the down-dip extension of the fault is the same as that of a fault loaded by far-field boundary conditions with no localized slip at depth. The periodicity of the rupture sequence

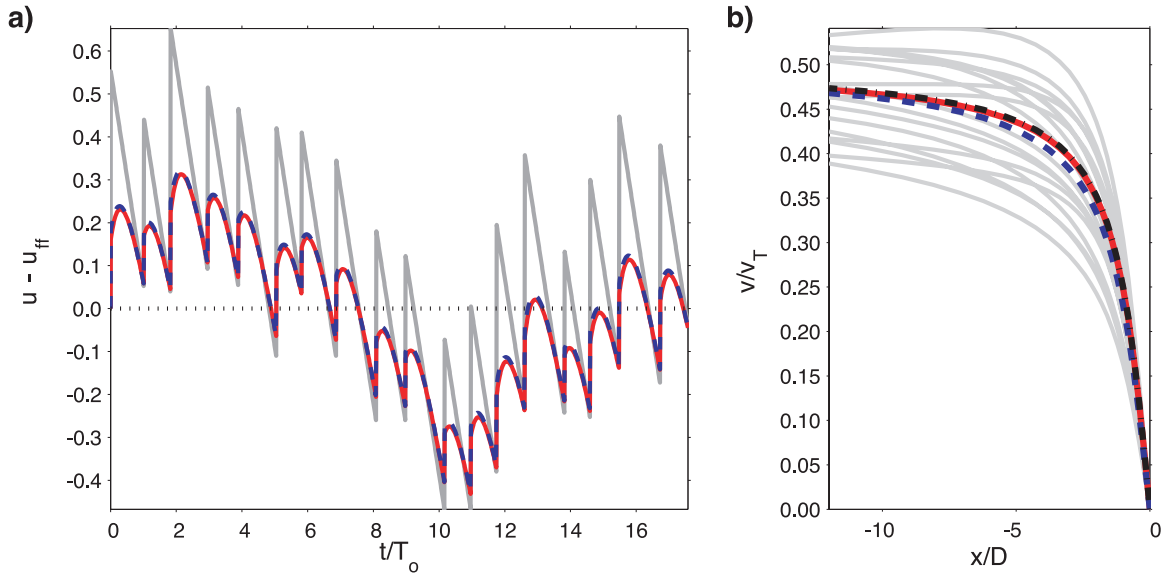

Figure C1. (a) Displacements relative to the far-field ($u - u_{\mathrm{ff}}$) through mature seismic cycles $2D$ from a fault in a one-layer model with Maxwell rheologies ($\mu_c = \mu$, $\tau_o = T_o|\alpha_1| = 5$) and the fault loaded by deep steady-slip (red solid line) and by far-field shear (blue dashed line). Also shown are the displacements at $x/D = 0^+$ (gray lines). Enough cycles are shown such that the cumulative deformation is nearly block-like. (b) Average interseismic velocities during the 18 cycles shown at left when the fault is loaded from below (red solid line) and from the far-field (blue dashed line) with the CEHM interseismic velocities (black dash-dot line). The average velocities in each of the 18 cycles are shown to indicate the variation of velocities over the sequence (gray lines).

can either be the periodic repetition of an individual rupture or a finite sequence of ruptures [*Hetland and Hager*, 2005].

[68] The mature interseismic velocities are also independent of fault loading during cycles within a nonperiodic rupture sequence not containing periodicity. We demonstrate this by comparing the mature interseismic deformation of two fault models, one with a fault loaded by far-field shear and the other loaded by steady-sliding on the downward extension of the randomly rupturing fault (Figure C1). We calculate the deformation in the models driven by far-field shear and from below using a finite element model and the analytic solution of *Hetland and Hager* [2005], respectively. In both models, the fault ruptures uniformly from the surface to depth D, and in the model loaded by far-field shear the fault slip also tapers to zero at depth $1.2D$ (see Appendix A for a description of the finite element models). We do not account for the slip taper in the analytic calculations, hence there is a geometric mismatch between the two models shown in Figure C1 (see *Hetland and Hager* [2005] for a discussion concerning the comparison of the analytic solution with finite element models). The additional fault taper in the finite element model results in larger coseismic displacements and lower interseismic velocities near the fault compared to the analytic model (Figure C1); however, allowing for this discrepancy, the mature deformation is the same in both fault loading models.

Notation

D	fault locking depth.
v_T	rate of fault loading.
T	rupture repeat time.
Δ	fault rupture offset.
$v_{\mathrm{sl}} = \Delta/T$	fault slip rate.
μ	Maxwell shear modulus.
$\tau_M = \eta_M/\mu_M$	Maxwell viscoelastic relaxation time (η_M and μ_M is the Maxwell viscosity and shear modulus, respectively).
$\tau_o = T/2\tau_M = T\lvert\alpha_1\rvert$	the Savage parameter.
$\lvert\alpha_i\rvert^{-1}$	mechanical relaxation timescale [*Hetland and Hager*, 2005].

$|\alpha_{st}|^{-1} = \tau_{st}$ ($|\alpha_{tr}|^{-1} = \tau_{tr}$) mechanical relaxation time associated with the steady (transient), nonrecoverable (recoverable) phase of postseismic relaxation.

σ_f difference between the initial and the average mature shear stresses on a fault.

t_i time for the average shear stresses in each cycle to reach 0.9 σ_f.

$N_i = t_i/T$ number of seismic cycles for the average shear stresses in each cycle to reach 0.9 σ_f.

L distance from the fault to the model boundaries.

H thickness of the middle layer in a two-layer model.

λ distance between faults in a two-fault model.

Glossary

Classic elastic half-space model (CEHM): The interseismic deformation model of *Savage and Burford* [1973]: an infinite length, vertical strike-slip fault in an elastic half-space loaded by steady sliding on the extension of the fault below the locking depth.

Cycle-invariant state: The time when the interseismic surface deformation is the same in every seismic cycle, i.e., the mature state for a fault with a periodic rupture sequence.

Equivalent elastic model: An elastic model with the same geometry and distribution of elastic shear modulus as a viscoelastic model.

Fault loading: The mechanism that loads the fault.

Locking depth: Depth of the maximum coseismic rupture.

Mature state: The time following the adjustment to fault loading conditions and when the interseismic surface deformation no longer depend on the fault loading.

Phase variables of interseismic velocities: The apparent D and v_T of a CEHM (equation (1)) fit to the interseismic velocities.

Primary velocities: The average mature interseismic velocities over a time window such that the deformation is block-like, also the velocities of the equivalent elastic model.

Rupture sequence: Time history of fault ruptures, a periodic rupture sequence is a sequence where ruptures of constant magnitude repeat regularly in time.

Savage parameter: The ratio of the average rupture repeat time to the mechanical relaxation time due to the steady coupling of the upper faulted layer to the lower region.

Seismic cycle: The period including a fault rupture up until the next rupture.

Slip rate: The rupture offset divided by the rupture repeat time.

Spin-up: The time during which a fault system transitions from the initial to mature states.

Standard model of interseismic deformation: The model of Savage and colleagues [*Savage and Prescott*, 1978; *Savage and Lisowski*, 1998; *Savage*, 2000]: an infinite length, vertical strike-slip fault, loaded by steady-sliding on the extension of the fault at depth and rupturing periodically, in an elastic layer overlying a Maxwell viscoelastic half-space.

Acknowledgments

[69] We thank Roland Bürgmann and Mousumi Roy for their exceptionally thorough and insightful reviews of this paper; their comments, along with those of the Associate Editor James Gaherty and the Editor Peter van Keken, greatly improved this paper. Additionally, this paper benefited from discussions with B. Meade, and we thank S. Kenner and M. Simons for an advance copy of their paper. We thank G. Lyzenga and J. Parker for the use of GeoFEST. We used Matlab (The Mathworks, Inc.) to generate all figures presented in this paper. This research was supported by NSF grant EAR-0346021.

References

Bonafede, M., M. Dragoni, and A. Morelli (1986), On the existence of a periodic dislocation cycle in horizontally layered viscoelastic models, *J. Geophys. Res.*, *91*, 6396–6404.

Bott, M. H. P., and S. Dean (1973), Stress diffusion from plate boundaries, *Nature*, *243*, 339–341.

Bourne, S. J., P. C. England, and B. Parsons (1998), The motion of crustal blocks driven by flow of the lower lithosphere and implications for slip rates of continental strike-slip faults, *Nature*, *391*, 655–659.

Bowman, D., G. King, and P. Tapponnier (2003), Slip partitioning by elastoplastic propagation of oblique slip at depth, *Science*, *300*, 1121–1123.

Bürgmann, R., S. Ergintav, P. Segall, E. H. Hearn, S. McClusky, R. E. Reilinger, H. Woith, and J. Zschau (2002), Time-dependent afterslip on and deep below the İzmit earthquake rupture, *Bull. Seismol. Soc. Am.*, *92*, 126–137.

Chèry, J., S. Merkel, and S. Bouissou (2001), A physical basis for time clustering of large earthquakes, *Bull. Seismol. Soc. Am.*, *91*, 1685–1693.

Chinnery, M. A., and D. B. Jovanovich (1972), Effect of Earth layering on earthquake displacement fields, *Bull. Seismol. Soc. Am.*, *62*, 1629–1639.

DiCaprio, C. J., M. Simons, S. J. Kenner, and C. A. Williams (2004), Temporal clustering of earthquakes due to stress transfer in viscoelastic layers, *Eos Trans. AGU*, *85*(47), G13A-0784.

Dixon, T. H., E. Norabuena, and L. Hotaling (2003), Paleoseismology and global positioning system: Earthquake-cycle effects and geodetic versus geologic fault slip rates in the Eastern California shear zone, *Geology*, *31*, 55–58.

Dolan, J. F., K. Sieh, T. K. Rockwell, R. S. Yeats, J. Shaw, J. Suppe, G. J. Huftile, and E. M. Gath (1995), Prospects for larger or more frequent earthquakes in the Los Angeles metropolitan region, *Science*, *267*, 199–205.

Fay, N. P., and E. D. Humphreys (2005), Fault slip rates, effects of elastic heterogeneity on geodetic data, and the strength of the lower crust in the Salton Trough region, southern California, *J. Geophys. Res.*, *110*, B09401, doi:10.1029/2004JB003548.

Freed, A. M., and R. Bürgmann (2004), Evidence of power-law flow in the Mojave desert mantle, *Nature*, *430*, 548–551.

Grant, L. B., and K. Sieh (1994), Paleoseismic evidence of clustered earthquakes on the San Andreas fault in the Carrizo Plain, California, *J. Geophys. Res.*, *99*, 6819–6841.

Hearn, E. H., R. Bürgmann, and R. E. Reilinger (2002), Dynamics of İzmit earthquake postseismic deformation and loading of the Düzce earthquake hypocenter, *Bull. Seismol. Soc. Am.*, *92*, 172–193.

Hetland, E. A., and B. H. Hager (2003), Postseismic relaxation across the Central Nevada Seismic Belt, *J. Geophys. Res.*, *108*(B8), 2394, doi:10.1029/2002JB002257.

Hetland, E. A., and B. H. Hager (2004), Relationship of geodetic velocities to velocities in the mantle, *Geophys. Res. Lett.*, *31*, L17604, doi:10.1029/2004GL020691.

Hetland, E. A., and B. H. Hager (2005), Postseismic and interseismic displacements near a strike-slip fault: A two-dimensional theory for general linear viscoelastic rheologies, *J. Geophys. Res.*, *110*, B10401, doi:10.1029/2005JB003689.

Hetland, E. A., and B. H. Hager (2006), The effects of rheological layering on postseismic deformation, *Geophys. J. Int.*, in press.

Hilley, G. E., R. Bürgmann, P. Z. Zhang, and P. Molnar (2005), Bayesian inference of plastosphere viscosities near the Kunlun Fault, northern Tibet, *Geophys. Res. Lett.*, *32*, L01302, doi:10.1029/2004GL021658.

Ivins, E. R. (1996), Transient creep of a composite lower crust: 2. A polymineralic basis for rapidly evolving postseismic deformation modes, *J. Geophys. Res.*, *101*, 28,005–28,028.

Jackson, J. (2002), Faulting, flow, and the strength of the continental lithosphere, *Int. Geol. Rev.*, *44*, 39–61.

Johnson, K. M., and P. Segall (2004), Viscoelastic earthquake cycle models with deep stress-driven creep along the San Andreas fault system, *J. Geophys. Res.*, *109*, B10403, doi:10.1029/2004JB003096.

Kenner, S. J., and M. Simons (2005), Temporal clustering of major earthquakes along individual faults due to post-seismic reloading, *Geophys. J. Int.*, *160*, 179–194, doi:10.1111/j.1365-246X.2005.02460.x.

Lay, T., and T. C. Wallace (1995), *Modern Global Seismology*, 521 pp., Elsevier, New York.

Li, V. C., and J. R. Rice (1987), Crustal deformation in great California earthquake cycles, *J. Geophys. Res.*, *92*, 11,533–11,551.

Lynch, J. C., R. Bürgmann, and M. A. Richards (2003), When faults communicate: Viscoelastic coupling and earthquake clustering in a simple two-fault system, *Geophys. Res. Lett.*, *30*(6), 1270, doi:10.1029/2002GL016765.

Lyzenga, G. A., A. Raefsky, and S. G. Mulligan (1991), Models of recurrent strike-slip earthquake cycles and the state of crustal stress, *J. Geophys. Res.*, *96*, 21,623–21,640.

Lyzenga, G. A., W. R. Panero, and A. Donnellan (2000), Influence of anelastic surface layers on postseismic thrust fault deformation, *J. Geophys. Res.*, *105*, 3151–3157.

Meade, B. J., and B. H. Hager (2004), Viscoelastic deformation for a clustered earthquake cycle, *Geophys. Res. Lett.*, *31*, L10610, doi:10.1029/2004GL019643.

Meade, B. J., and B. H. Hager (2005a), Block models of crustal motion in southern California constrained by GPS measurements, *J. Geophys. Res.*, *110*, B03403, doi:10.1029/2004JB003209.

Meade, B. J., and B. H. Hager (2005b), Spatial localization of moment deficits in southern California, *J. Geophys. Res.*, *110*, B04402, doi:10.1029/2004JB003331.

Montèsi, L. G. J. (2004), Controls of shear zone rheology and tectonic loading on postseismic creep, *J. Geophys. Res.*, *109*, B10404, doi:10.1029/2003JB002925.

Peltzer, G., F. Crampé, S. Hensley, and P. Rosen (2001), Transient strain accumulation and fault interaction in the Eastern California shear zone, *Geology*, *29*, 975–978.

Piersanti, A., G. Spada, R. Sabadini, and M. Bonafede (1995), Global post-seismic deformation, Geophys, *J. Int.*, *120*, 544–566.

Pollitz, F. F. (2001), Viscoelastic shear zone model of a strike-slip earthquake cycle, *J. Geophys. Res.*, *106*, 26,541–26,560.

Pollitz, F. F. (2003a), The relationship between the instantaneous velocity field and the rate of moment release in the lithosphere, *Geophys. J. Int.*, *153*, 595–608, doi:10.1046/j.1365-246X.2003.01924.x.

Pollitz, F. F. (2003b), Transient rheology of the uppermost mantle beneath the Mojave Desert, California, *Earth Planet Sci. Lett.*, *215*, 89–104.

Pollitz, F. F., and M. Nyst (2005), A physical model for strain accumulation in the San Francisco Bay region, *Geophys. J. Int.*, *160*, 302–317, doi:10.1111/j.1365-246X.2005.02433.x.

Pollitz, F. F., C. Wicks, and W. Thatcher (2001), Mantle flow beneath a continental strike-slip fault: Postseismic deformation after the 1999 Hector Mine earthquake, *Science*, *293*, 1814–1818.

Roy, M., and L. H. Royden (2000), Crustal rheology and faulting at strike-slip plate boundaries: 2. Effects of lower crustal flow, *J. Geophys. Res.*, *105*, 5599–5613.

Rybicki, K. (1971), The elastic residual field of a very long strike-slip fault in the presence of a discontinuity, *Bull. Seismol. Soc. Am.*, *61*, 79–92.

Sauber, J., W. Thatcher, S. C. Solomon, and M. Lisowski (1994), Geodetic slip rate for the eastern California shear zone and the recurrence time of Mojave desert earthquakes, *Nature*, *367*, 264–266.

Savage, J. C. (1990), Equivalent strike-slip earthquake cycles in halfspace and lithosphere-asthenosphere Earth models, *J. Geophys. Res.*, *95*, 4873–4879.

Savage, J. C. (2000), Viscoelastic-coupling model for the earthquake cycle driven from below, *J. Geophys. Res.*, *105*, 25,525–25,532.

Savage, J. C., and R. O. Burford (1973), Geodetic determination of relative plate motion in central California, *J. Geophys. Res.*, *78*, 832–845.

Savage, J. C., and M. Lisowski (1998), Viscoelastic coupling model of the San Andreas fault along the Big Bend, southern California, *J. Geophys. Res.*, *103*, 7281–7292.

Savage, J. C., and W. H. Prescott (1978), Asthenosphere readjustment and the earthquake cycle, *J. Geophys. Res.*, *83*, 3369–3376.

Scholz, C. H. (1998), Earthquakes and friction laws, *Nature*, *391*, 37–42.

Segall, P. (2002), Integrating geologic and geodetic estimates of slip rate on the San Andreas fault system, *Int. Geol. Rev.*, *44*, 62–82.

Sharp, R. V. (1981), Variable rates of late quaternary strike slip rates on the San Jacinto fault zone, *J. Geophys. Res.*, *86*, 1754–1762.

Smith, B., and D. Sandwell (2004), A three-dimensional semi-analytic viscoelastic model for time-dependent analysis of the earthquake cycle, *J. Geophys. Res.*, *109*, B12401, doi:10.1029/2004JB003185.

Vergnolle, M., F. Pollitz, and E. Calais (2003), Constraints on the viscosity of the continental crust and mantle from GPS measurements and postseismic deformation models in western Mongolia, *J. Geophys. Res.*, *108*(B10), 2502, doi:10.1029/2002JB002374.

Wallace, R. E. (1987), Grouping and migration of surface faulting and variations in slip rates on faults in the Great Basin province, *Bull. Seismol. Soc. Am.*, *77*, 868–876.

Weldon, R. J., and K. E. Sieh (1985), Holocene rate of slip and tentative recurrence interval for large earthquakes on the San Andreas fault, Cajon Pass, southern California, *Geol. Soc. Am. Bull.*, *96*, 793–812.

Weldon, R., T. Fumal, and G. Biasi (2004), Wrightwood and the earthquake cycle: What a long recurrence record tells us about how faults work, *GSA Today*, *14*(9), 2, doi:10.1130/1052-5173(2004)014<4:WATECW>2.0.CO.

Zatman, S. (2000), On steady rate coupling between an elastic upper crust and a viscous interior, *Geophys. Res. Lett.*, *27*, 2421–2424.